

Research

---

# Assessment of Fuel Rod Failure Thresholds for Reactivity Initiated Accidents

Lars Olof Jernkvist  
Ali R. Massih

November 2004

# **SKI Perspective**

## **Background and purpose of the project**

Over the last 10 years the behaviour of nuclear fuel during reactivity initiated accidents has been studied to investigate the failure threshold as a function of burnup. Experimental programmes performed in the CABRI test reactor (France) and in the Nuclear Safety Research Reactor (Japan) have indicated that cladding failure and fuel dispersion of high burnup fuel may occur at enthalpy values lower than previously estimated.

At the beginning of 1995 SKI issued fuel and cladding failure limits based on available test data. It was envisaged at that time that the failure limits should be re-evaluated when more information was available. Since then SKI has joined the OECD-IRSN CABRI water loop project at the end of 2000. The purpose was to gain information on the failure threshold for nuclear fuel cladding as a function of burnup, especially for modern cladding materials and during prototypical conditions.

In 2003 SKI initiated a study, in cooperation with the Swedish nuclear utilities, to recommend more relevant fuel failure limits for reactivity initiated accidents.

The work presented in this report is the second part of the study. In the report failure thresholds are calculated by use of best-estimate computational methods. In the first part a strain-based failure criterion was formulated based on mechanical tests and compared with experimental tests and other failure criterion. This is reported in SKI report 2004:32. The third part is a sensitivity study which is reported in SKI report 2004:34.

## **Results**

This project has contributed to the research goal of giving a basis for SKI's supervision by means of evaluating and modelling the nuclear fuel cladding failure threshold during a design base accident. The project has also contributed to the research goal to develop the competence about licensing of fuel at high burnup, which is an important safety issue.

## **Project information**

Responsible for the project at SKI has been Jan in de Betou.  
SKI Reference: 14.06-011070/02149

## Research

---

# Assessment of Fuel Rod Failure Thresholds for Reactivity Initiated Accidents

Lars Olof Jernkvist  
Ali R. Massih

Quantum Technologies AB  
Uppsala Science Park  
SE-751 83 Uppsala  
Sweden

November 2004

This report concerns a study which has been conducted for the Swedish Nuclear Power Inspectorate (SKI). The conclusions and viewpoints presented in the report are those of the author/authors and do not necessarily coincide with those of the SKI.

# List of contents

Summary.....	III
Sammanfattning.....	IV
1 Introduction .....	1
2 Analyses .....	3
2.1 Scope of analyses .....	3
2.2 Computational models and methods .....	4
2.2.1 Computer codes .....	4
2.2.2 Computational procedure .....	4
2.2.3 Specific models introduced for the present analyses.....	5
2.3 Input.....	7
2.3.1 Fuel rod design .....	7
2.3.2 Steady-state base irradiation.....	7
2.3.3 Postulated reactivity initiated accidents .....	8
3 Results .....	11
3.1 Calculated fuel rod conditions prior to RIA .....	11
3.1.1 Clad corrosion .....	11
3.1.2 Pellet-clad gap conditions.....	13
3.2 Calculated fuel rod conditions under RIA.....	15
3.2.1 Fuel rod failure thresholds.....	15
3.2.2 Clad conditions at failure.....	16
3.2.3 Clad maximum temperature and deformation.....	18
4 Discussion.....	21
4.1 Applicability of calculated failure thresholds.....	21
4.2 Evaluation of calculated fuel rod failure thresholds.....	23
4.2.1 Comparison with current fuel rod failure threshold .....	23
4.2.2 Comparison with similar studies .....	26
4.2.3 Comparison with pulse test data.....	29
4.3 Sensitivity studies .....	30
4.3.1 Impact of uncertainty in clad failure prediction .....	30
4.3.2 Impact of clad corrosion.....	31
4.3.3 Impact of clad oxide spallation under RIA.....	34
5 Conclusions .....	37
6 References .....	39

# List of appendices

Appendix A:	
Current fuel rod failure threshold for RIA in Sweden.....	43
Appendix B:	
Power histories and axial power distributions applied in simulations of base irradiation .....	44
Appendix C:	
Calculated fuel rod failure conditions under PWR HZP REA .....	45
Appendix D:	
Calculated fuel rod failure conditions under BWR CZP CRDA.....	46
Appendix E:	
Calculated impact of clad corrosion on clad temperature and hoop plastic strain at failure.....	47
Appendix F:	
Calculated impact of clad oxide transient spallation on clad temperature and hoop plastic strain at failure.....	49

## Summary

Failure thresholds for high-burnup light water reactor  $\text{UO}_2$  fuel rods, subjected to postulated reactivity initiated accidents (RIAs), are here assessed by use of best-estimate computational methods. The considered RIAs are the hot zero power rod ejection accident (HZP REA) in pressurized water reactors and the cold zero power control rod drop accident (CZP CRDA) in boiling water reactors. Failure thresholds for these events, formulated in terms of allowable fuel enthalpy with respect to fuel burnup, are calculated for fuel burnups ranging from 30 to 70  $\text{MWd}(\text{kgU})^{-1}$ . The calculations are performed with best-estimate models, applied in the FRAPCON-3.2 and SCANAIR-3.2 computer codes. Fuel rod integrity under RIA is assessed by use of a strain-based clad failure criterion, which is formulated specifically for the performed analyses. The criterion is intended for best-estimate prediction of clad tube failure, caused by pellet-clad mechanical interaction under the early heat-up phase of an RIA.

Supported by the results of three-dimensional core kinetics analyses, the considered RIA power pulses are simulated by a Gaussian line shape, with a fixed width of either 25 ms (REA) or 45 ms (CRDA). Notwithstanding the differences in postulated accident scenarios between the REA and the CRDA, the calculated fuel rod failure thresholds for these two events are similar. The calculated failure enthalpy decreases gradually with fuel burnup, from approximately  $650 \text{ J}(\text{gUO}_2)^{-1}$  at  $30 \text{ MWd}(\text{kgU})^{-1}$  to  $530 \text{ J}(\text{gUO}_2)^{-1}$  at  $70 \text{ MWd}(\text{kgU})^{-1}$ . Calculated clad temperatures and hoop plastic strains at time of clad failure are typically 800-900 K and 1.2-1.6 %, respectively, for both the REA and the CRDA. Calculated hoop strain rates at failure are  $0.6\text{-}0.9 \text{ s}^{-1}$  for the considered REA and  $0.2\text{-}0.5 \text{ s}^{-1}$  for the CRDA.

Parametric sensitivity studies are performed in addition to the best-estimate analyses, in order to estimate uncertainties in calculated results, and also to identify key parameters and models in the analyses. These sensitivity studies indicate that the pulse width may have a significant impact on the failure enthalpy, at least for pulses narrower than 50 ms. Clad corrosion seems on the other hand to be of minor importance to the failure enthalpy, as long as the clad oxide layer is non-spalled and possible hydrides in the material are uniformly distributed. However, for cladding tubes with spalled oxide, the ductility of the material may be dramatically reduced as a consequence of non-uniform hydride precipitation, and the failure threshold significantly lower. The calculated failure enthalpy for PWR fuel rods with spalled oxide, subjected to the postulated HZP REA, is approximately  $350 \text{ J}(\text{gUO}_2)^{-1}$  at a fuel burnup of  $65 \text{ MWd}(\text{kgU})^{-1}$ .

In conclusion, the performed analyses indicate that a common fuel rod failure threshold for HZP REA and CZP CRDA, expressed in terms of allowable fuel enthalpy with respect to fuel burnup, is feasible, provided that the threshold is applied to fuel rods with non-spalled clad oxide.

## Sammanfattning

I denna rapport används realistiska beräkningsmodeller för att fastställa bränsleskadegränser gällande högutbrända  $\text{UO}_2$ -bränslestavar under postulerade reaktivitetsinitierade olyckor (RIA) i lättvattenreaktorer. Två skilda reaktivitetsolyckor beaktas: styrstavsutskjutning vid nolleffekt och varm härd (HZP REA) i tryckvattenreaktorer, samt fallande styrstav vid nolleffekt och kall härd (CZP CRDA) i kokvattenreaktorer. För dessa två fall beräknas bränsleskadegränser, vilka här definieras i form av maximal tillåten bränsleentalpi vid given utbränning, i intervallet 30 till 70  $\text{MWd}(\text{kgU})^{-1}$ . För beräkningarna används "best-estimate"-modeller i beräkningsprogrammen FRAPCON-3.2 och SCANAIR-3.2. Bränslestavskador under RIA predikteras med ett härför framtaget töjningsbaserat skadekriterium för kapslingsröret. Kriteriet är avsett för prediktering av kapslingsrörsskador orsakade av mekanisk växelverkan mellan kuts och kapslingsrör vid uppvärmningsförloppet under reaktivitetsolyckans initialfas.

Baserat på resultat av tredimensionella härdkinetikanalyser ansättes en Gaussformad effektpuls med en pulsvidd om antingen 25 ms (REA) eller 45 ms (CRDA) för att simulera reaktivitetsolyckan. Trots skillnaderna i postulerade förlopp för de två beaktade olyckorna, så är de beräknade bränsleskadegränserna likartade för de två fallen. Den beräknade tröskelentalpin för bränsleskada avtar gradvis med ökande utbränning, från omkring  $650 \text{ J}(\text{gUO}_2)^{-1}$  vid  $30 \text{ MWd}(\text{kgU})^{-1}$  till  $530 \text{ J}(\text{gUO}_2)^{-1}$  vid  $70 \text{ MWd}(\text{kgU})^{-1}$ . Beräknade kapslingstemperaturer och plastiska ringtöjningar vid brott är typiskt 800-900 K respektive 1.2-1.6 %, vilket gäller för båda två av de beaktade fallen. Beräknade ringtöjningshastigheter vid brott är  $0.6-0.9 \text{ s}^{-1}$  för REA och  $0.2-0.5 \text{ s}^{-1}$  för CRDA.

Känslighetsanalyser med avseende på utvalda parametrar genomförs som komplement till "best-estimate"-beräkningarna, dels i syfte att uppskatta osäkerheter i beräkningsresultaten, dels för att identifiera nyckelparametrar och modeller. Dessa känslighetsanalyser visar att pulsvidden kan ha en betydande inverkan på tröskelentalpin för bränsleskada, åtminstone för effektpulser kortare än 50 ms. Kapslingsrörets korrosion verkar å andra sidan vara av mindre betydelse för tröskelentalpin, under förutsättning att kapslingens oxid ej är flagad och eventuella hydrider är jämnt fördelade i materialet. I kapslingsrör med flagad oxid kan emellertid materialets duktilitet minska avsevärt på grund av ojämn hydridansamling, vilket resulterar i betydligt lägre tröskelentalpier. Den beräknade tröskelentalpin för flagade bränslestavar av tryckvattenreakortyp, utsatta för den postulerade reaktivitetsolyckan, är cirka  $350 \text{ J}(\text{gUO}_2)^{-1}$  vid en utbränning av  $65 \text{ MWd}(\text{kgU})^{-1}$ .

Med stöd av de genomförda analyserna finner vi det möjligt att definiera en gemensam bränsleskadegräns för HZP REA och CZP CRDA, uttryckt i maximal tillåten bränsleentalpi vid given utbränning, under förutsättning att bränsleskadegränsen tillämpas på bränslestavar med icke flagad oxid.

# 1 Introduction

The work presented in this report is the final part of a two-step project, which is aimed at establishing failure thresholds for high-burnup light water reactor fuel rods under reactivity initiated accidents (RIAs). The mechanisms responsible for clad tube failure under RIA in high-burnup fuel were studied in the first part of the project, and a strain-based clad failure criterion was formulated from more than 200 out-of-pile mechanical property tests (Jernkvist et al., 2004). In the present report, this failure criterion is applied in best-estimate computer analyses of postulated RIAs, and burnup-dependent fuel rod failure thresholds in terms of allowable fuel enthalpy are calculated.

The calculated fuel rod failure thresholds should not be viewed as definite operational limits, but merely as assessments of the influence of fuel rod burnup, clad corrosion, cooling conditions, power pulse shape and other parameters on the propensity for clad tube failure under RIA. Such analytical assessments are needed, when evaluating experimental failure/no-failure data from pulse reactor tests. This is due to the fact that large differences exist between the samples (fuel design, clad corrosion) as well as between the pulse reactor test facilities (power pulse width, cooling conditions). These differences make it difficult to establish burnup-dependent failure thresholds by direct rendition of the pulse reactor test data. Analytical tools are generally needed in order to interpret the tests, and also to correctly transform the results from non-prototypical pulse reactor conditions to typical light water reactor conditions. To this end, it should be noticed that the current fuel failure threshold for RIA in Sweden is based on direct rendition of data from pulse reactor tests (SKI, 1995). This fuel failure threshold, established by the Swedish Nuclear Power Inspectorate (SKI) in 1995, is shown together with its supporting experimental data in appendix A.

In this report, fuel rod failure thresholds are calculated for two hypothetical reactivity initiated accidents in light water reactors: the hot zero power rod ejection accident in pressurized water reactors, and the cold zero power control rod drop accident in boiling water reactors. The calculated failure thresholds for these two events are defined in terms of allowable fuel enthalpy with respect to burnup in the range from 30 to 70  $\text{MWd}(\text{kgU})^{-1}$ . The calculations are performed with best-estimate computational models, but conservative assumptions are made in input to the analyses, in order to account for the uncertainties associated with high-burnup fuel rod behaviour under fast power transients. The best-estimate analyses are also supplemented with parametric sensitivity studies, in order to estimate the uncertainty in the calculated failure thresholds.

The organization of the report is as follows:

The computational models and methods applied in analyses are described in section 2, together with the assumptions made about fuel rod design, steady-state base irradiation conditions and the postulated reactivity initiated accidents.

Section 3 contains the results of the performed analyses. Calculated burnup-dependent fuel rod conditions prior to RIA, such as clad corrosion and pellet-clad gap conditions, are first presented in section 3.1. These calculated conditions serve as input to the analyses of the actual RIA, the results of which are compiled in section 3.2. Here, the calculated fuel rod failure thresholds are presented, together with data on key fuel rod properties, such as clad temperatures and deformations under the power excursion.

The calculated fuel rod failure thresholds are discussed and evaluated in section 4 of the report, where comparisons are made with experimental data and the current fuel rod failure threshold for RIA in Sweden. Comparisons are also made with other calculated failure thresholds for high-burnup pressurized water reactor fuel, which have recently been presented at international conferences. Finally, our calculated failure thresholds are discussed in light of parametric sensitivity studies, which were performed in order to assess the impact of pulse width, cooling conditions, clad corrosion and oxide transient spallation on the propensity for fuel rod failure under RIA.

## 2 Analyses

### 2.1 Scope of analyses

The hypothetical reactivity initiated accidents considered in this report are the hot zero power (HZP) rod ejection accident (REA) in pressurized water reactors (PWRs) and the cold zero power (CZP) control rod drop accident (CRDA) in boiling water reactors (BWRs). In both these scenarios, mechanical failure of a control rod drive mechanism leads to a prompt power excursion, which initiates from near zero power conditions and terminates by negative feedback from the fuel temperature rise (Doppler effect). The power pulse widths considered in analyses are 25 ms for the HZP REA and 45 ms for the CZP CRDA; see section 2.3.3 for further details on the assumptions made about the reactivity initiated accidents.

The thermo-mechanical response of typical PWR and BWR fuel rods to these transients is analysed, using best-estimate computational models. Best-estimate fuel rod failure thresholds for HZP REA and CZP CRDA, in terms of maximum allowable fuel enthalpy, are calculated for fuel burnups in the range from 30 to 70 MWd(kgU)<sup>-1</sup>. The upper end of this interval corresponds to the highest burnups, for which the computer codes and models applied in analyses have been verified with experimental data (Lanning et al., 1997). The lower end of the interval is the burnup about which a transition in clad failure mode is observed in pulse reactor tests (Jernkvist et al., 2004). Failure of low-burnup fuel rods usually occurs after excessive clad deformation (ballooning) at high clad temperatures, whereas high-burnup failures may occur already at low clad temperatures under the early heat-up phase of the RIA. In this case, the clad tube fails after moderate deformation, resulting from pellet-clad mechanical interaction (PCMI). In this report, we consider fuel burnups between 30 and 70 MWd(kgU)<sup>-1</sup>, for which the PCMI-induced failure mode is believed to be more restricting than the high-temperature failure mode.

The computational models and methods are described in section 2.2 below, whereas the fuel designs are defined in section 2.3.1. The applicability of the calculated failure thresholds is discussed in section 4.1, where also the limitations of the performed analyses are defined. To this end, it should be noticed that the analyses are restricted to UO<sub>2</sub> fuel rods, and that the considered clad tube materials are standard stress relieved annealed Zircaloy-4 and standard recrystallized Zircaloy-2 for the PWR and BWR fuel rod, respectively.

## 2.2 Computational models and methods

### 2.2.1 Computer codes

The fuel rod thermo-mechanical behaviour under RIA is analysed by use of the SCANAIR-3.2 computer code (Federici et al., 2000). Since SCANAIR lacks models for simulation of long-term steady-state irradiation, the SKI-version of the FRAPCON-3.2 steady-state fuel performance code is used to establish burnup-dependent initial conditions to the transient analyses (Berna et al., 1997). This version of FRAPCON-3.2 is equipped with an interface to SCANAIR-3.2 (Jernkvist, 2002). Both SCANAIR and FRAPCON are best-estimate computational tools, and throughout the performed analyses, the computer codes are used with their default best-estimate models. For the purpose of our analyses, however, some specific models are added to the codes. These models are described in section 2.2.3 below.

### 2.2.2 Computational procedure

The computer codes described above are used for determining burnup-dependent fuel rod failure thresholds in terms of maximum allowable fuel pellet enthalpy for PWR HZP REA and BWR CZP CRDA. Both thresholds are determined by the same procedure, as illustrated in figure 2.1. First, a generic base irradiation history is simulated by FRAPCON-3.2 up to a desired fuel burnup, in order to generate burnup-dependent fuel rod initial conditions needed for transient analysis with SCANAIR-3.2. With these initial conditions, SCANAIR is then used to analyse the fuel rod response to a reactivity initiated event, which is represented by a Gaussian power pulse with a fixed width of either 25 ms (PWR) or 45 ms (BWR). These pulse widths are selected, based on the results of three-dimensional core kinetics analyses of RIA, as described in section 2.3.3. The pulse amplitude is taken as a free parameter, and SCANAIR is run in an iterative loop in order to determine the pulse amplitude at which clad tube failure is predicted.

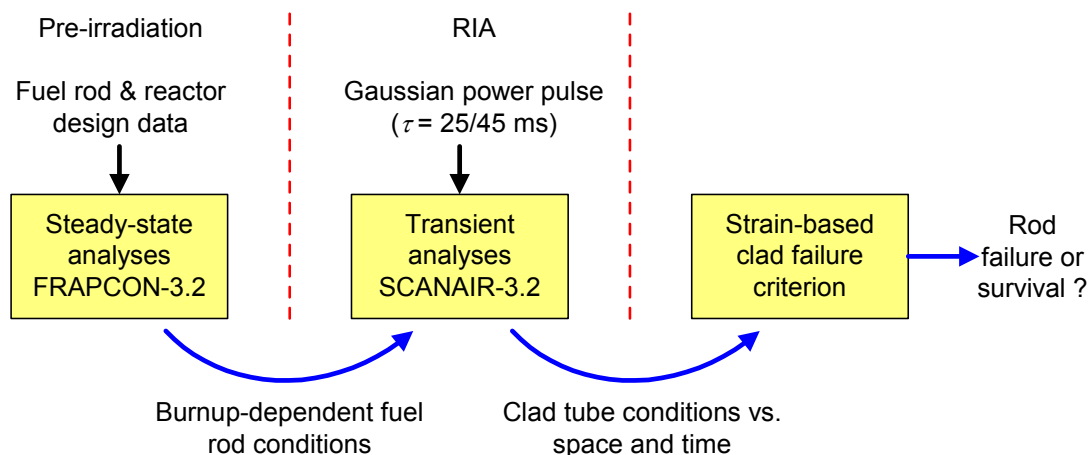


Figure 2.1: Computational procedure applied in analyses.

Once this critical pulse amplitude is found, iterations are terminated and the corresponding threshold fuel enthalpy is recorded in a diagram with respect to fuel burnup. By repeating this FRAPCON-SCANAIR analysis procedure for about 10 burnup levels in the range from 30 to 70 MWd(kgU)<sup>-1</sup>, the threshold fuel pellet enthalpy (peak radial average enthalpy under the pulse) is determined as a function of local burnup at the axial position of failure.

The full-length fuel rod is modelled in all analyses with FRAPCON and SCANAIR. The same axial discretization, consisting of 10 equal-length axial segments, is used for both computer codes.

## 2.2.3 Specific models introduced for the present analyses

### 2.2.3.1 Fuel pellet high-burnup rim properties

The models for fission gas release and pellet gas-induced deformations applied in the SCANAIR-3.2 computer code require detailed information about the burnup-dependent variation in material microstructure along the fuel pellet radius. Of particular interest is the formation of a characteristic high-burnup microstructure at the pellet periphery (rim zone), which starts at a pellet average burnup of approximately 40 MWd(kgU)<sup>-1</sup>. The formation of a high-burnup rim zone structure is not modelled in FRAPCON-3.2, and the microstructural data required for the rim zone by SCANAIR are therefore estimated from experimental studies reported in literature as follows:

The width of the rim zone,  $w_{Rim}$  [ $\mu\text{m}$ ], is in all analyses with SCANAIR correlated to the pellet radial average burnup,  $E_{av}$  [MWd(kgU)<sup>-1</sup>], through

$$w_{Rim} = \begin{cases} 0 & E_{av} \leq 35, \\ 4.27 \cdot 10^{-2} (E_{av} - 35)^{2.41} & 35 < E_{av} < 70. \end{cases} \quad (2.1)$$

Equation (2.1) is a fit to the optical microscopy data presented by Manzel and Walker (2000). The material within the rim zone is assumed to have a uniform microstructure, the properties of which are defined in table 2.1. These properties are compiled from several studies on rim zone formation, which have been reviewed by Jernkvist and Massih (2002a).

<b>Fuel material property</b>		<b>Rim zone</b>	<b>As-fabricated</b>
Density	[ kgm <sup>-3</sup> ]	9670	10250
Porosity (volume fraction)	[ - ]	0.10	0.04
Grain size	[ $\mu\text{m}$ ]	0.3	10
Intergranular bubble size	[ nm ]	2.0	20

*Table 2.1: Rim zone microstructural properties applied in analyses with SCANAIR-3.2. Typical properties of as-fabricated un-irradiated UO<sub>2</sub> fuel are also given for reference.*

### 2.2.3.2 Clad-to-coolant heat transfer

Models in the SCANAIR-3.2 computer code cater for heat transfer from the clad tube to the surrounding coolant, consisting of either liquid sodium or liquid water (Federici et al., 2000). For the purpose of our analyses, we have equipped SCANAIR-3.2 with an extended coolant channel model, allowing for two-phase flow and thus for simulations of BWR operating conditions. In the extended model, which is fashioned after the coolant channel model in the FRAPTRAN computer code (Cunningham et al., 2001), the two-phase water coolant is treated as a homogeneous mixture of liquid and steam in thermodynamic equilibrium. The model has an extended set of clad-to-water heat transfer correlations, which is applicable to both PWR and BWR conditions. In table 2.2, the new set of correlations is compared with the standard models for clad-to-water heat transfer in SCANAIR-3.2. Most of the correlations in table 2.2 are described in a review of heat transfer correlations for light water reactor application, recently published by the IAEA (2001).

<b>Heat transfer regime</b>	<b>Standard SCANAIR-3.2</b>	<b>Extended SCANAIR-3.2</b>
Forced convection to liquid phase	Dittus-Boelter	Dittus-Boelter
Subcooled nucleate boiling	Thom	Thom
Saturated nucleate boiling	-	Chen
Film boiling	Bishop-Sandberg-Tong	Groeneveld
Transition boiling	-	Condie-Bengtson
Forced convection to vapour phase	-	Dittus-Boelter
Critical heat flux	Babcock & Wilcox	EPRI-Columbia

*Table 2.2: Clad-to-water heat transfer correlations used in SCANAIR-3.2. For a description of these correlations, see (IAEA, 2001).*

### 2.2.3.3 Clad failure criterion

In order to assess fuel rod integrity under the postulated reactivity initiated accidents, a strain-based clad failure criterion has been implemented in SCANAIR-3.2. Clad tube failure is assumed to take place when the calculated clad hoop plastic strain (the relative permanent elongation in the clad circumferential direction) exceeds a threshold value, which is correlated to clad temperature, fast neutron fluence, hydrogen content, oxide layer thickness and strain rate on a best-estimate basis. The correlation for the threshold hoop plastic strain is derived from more than 200 out-of-pile mechanical property tests, made on irradiated clad tubes from fuel rods reaching burnups up to  $68 \text{ MWd}(\text{kgU})^{-1}$ , as well as on un-irradiated hydrogen-charged tube samples. A full description of this failure criterion and its experimental support can be found in (Jernkvist et al., 2004). The range of application of the failure criterion is summarized in section 4.1.

In analyses with SCANAIR, the failure criterion is applied to each of the 10 axial segments of the discretized fuel rod. However, clad failure is predicted always to occur at the axial position of peak clad corrosion, which is the 9<sup>th</sup> and 6<sup>th</sup> axial segment from the bottom of the rod for the PWR and BWR fuel rod, respectively. It should be noticed that the clad temperatures, strains and strain rates that are used in the clad failure criterion are radial average values.

## 2.3 Input

The input data to our thermo-mechanical analyses of postulated RIAs are partly based on core kinetics analyses, performed with the three-dimensional time-dependent neutronics code SIMULATE-3K by Vattenfall and OKG in an earlier part of this project, and we therefore apply much the same input as was used in these analyses. Hence, for the postulated rod ejection accident in PWRs, we assume the same fuel design and core conditions as applied by Gabrielson (2004) in analyses of HZP REA in Ringhals 3, a 3-loop PWR of Westinghouse design. For the postulated control rod drop accident in BWRs, we assume the same fuel design and core conditions as applied by Wiksell (2003) in analyses of CZP CRDA in Oskarshamn 3, an internal pump BWR of ASEA-ATOM design.

### 2.3.1 Fuel rod design

The fuel considered in analyses of PWR HZP REA is a 17×17 design (Gabrielson, 2004). In analyses of BWR CZP CRDA, the fuel design is 10×10 (Wiksell, 2003). The key properties of these fuel designs are summarized in table 2.3.

<b>Design parameter</b>	<b>PWR fuel rod 17×17</b>	<b>BWR fuel rod 10×10</b>
Fuel rod active length [ mm ]	3658	3680
Fuel rod pitch [ mm ]	12.6	13.0
Fuel rod fill gas	He	He
Fill gas pressure [MPa ]	2.50	0.60
Fuel pellet material	UO <sub>2</sub>	UO <sub>2</sub>
Fuel pellet density [ % of theoretical ]	95.0	96.7
U-235 enrichment [ % ]	3.80	4.00
Fuel pellet diameter [ mm ]	8.165	8.480
Pellet dish volume fraction [ % ]	1.40	1.12
Clad tube material	Zircaloy-4 (SRA)	Zircaloy-2 (RX)
Clad outer diameter [ mm ]	9.550	9.840
Clad wall thickness [ mm ]	0.610	0.605

*Table 2.3: Fuel rod designs considered in analyses.  
SRA: Stress relieved annealed. RX: Recrystallized.*

### 2.3.2 Steady-state base irradiation

The steady-state base irradiation is simulated by use of FRAPCON-3.2. Core cooling conditions corresponding to nominal conditions in the Ringhals 3 PWR and the Oskarshamn 3 BWR are assumed in these simulations; see table 2.4. The postulated steady-state power histories and axial power distributions are given in appendix B. The axial power distributions are assumed not to change during the irradiation history.

For the PWR fuel rod, a rod average linear heat generation rate (LHGR) of  $23 \text{ kWm}^{-1}$  is assumed for the first 290 effective full power days of operation, followed by a linear decrease in power with time, ending at  $8.73 \text{ kWm}^{-1}$  after 2000 days of reactor operation. A similar base irradiation is assumed for the BWR fuel rod: following 250 effective full power days at a constant rod average LHGR of  $25 \text{ kWm}^{-1}$ , the power decreases linearly with time, ending at  $8.17 \text{ kWm}^{-1}$  after 1800 days.

<b>Parameter</b>		<b>PWR</b>	<b>BWR</b>
Nominal thermal power	[ MW ]	2775	3020
Average linear heat generation rate	[ $\text{kWm}^{-1}$ ]	18.3	12.7
Coolant pressure	[ MPa ]	15.5	7.0
Coolant inlet temperature	[ K ]	557	550
Subchannel mass flow	[ $\text{gs}^{-1}$ ]	327.5	174.6
Subchannel mass flux	[ $\text{kg}(\text{m}^2\text{s})^{-1}$ ]	3759	1878

*Table 2.4: Core conditions applied in simulations of fuel rod base irradiation. These are nominal conditions of the Ringhals 3 and Oskarshamn 3 power plants, respectively. The coolant subchannel pertains to a single fuel rod.*

### 2.3.3 Postulated reactivity initiated accidents

The assumptions made about the reactivity initiated accidents in our analyses with SCANAIR-3.2 are based on the results of three-dimensional core kinetics analyses reported by Gabrielson (2004) and Wiksell (2003). Their analyses of postulated RIAs with SIMULATE-3K provided a spectrum of power pulses, with large variations in shape. This is illustrated in figures 2.2 and 2.3, which show calculated pulse widths and normalized pulse shapes from the analyses of HZP REA and CZP CRDA mentioned above (In de Betou et al., 2004).

To avoid the use of multiple pulse shapes in analyses of the thermo-mechanical fuel rod behaviour under RIA, a Gaussian power pulse is used in all analyses with SCANAIR. As shown in figure 2.3, the Gaussian pulse constitutes an envelop to the calculated pulse shapes, and it leads to conservative estimates of fuel rod failure enthalpies when applied in fuel rod analyses (Jernkvist, 2004). Moreover, the full width at half maximum of the applied Gaussian power pulse is set to 25 ms in analyses of HZP REA and to 45 ms in analyses of CZP CRDA. These pulse widths are taken from the lower end of the results presented in figure 2.2.

The core conditions applied under RIA are defined in table 2.5. They are identical to the conditions used by Gabrielson (2004) and Wiksell (2003). It should be noticed that the very low initial rod power leads to clad tube temperatures, prior to RIA, that are very close to the coolant temperature.

The distributions of generated power along the fuel rod under the considered RIAs are prescribed in a conservative manner, and do not reflect the true power distribution. The axial power distributions postulated for the PWR HZP REA and the BWR CZP CRDA in our analyses are shown in figure 2.4. The power distributions, which are assumed not to change during the transient, closely follow the calculated axial variations in clad oxide layer thickness along the fuel rods. Accordingly, the peak power under RIA is concentrated at the axial position of peak clad corrosion, and hence, at the weakest part of the clad tube. As a consequence of these conservatively assumed axial power distributions, clad failure is predicted always to occur at the axial position of peak clad corrosion. Moreover, peak fuel temperatures and enthalpies are also obtained at this position.

Parameter	PWR HZP REA	BWR CZP CRDA
Initial power [ % of nominal ]	0.1	0.01
Coolant pressure [ MPa ]	15.5	0.1
Coolant inlet temperature [ K ]	564.9	303.1
Subchannel mass flow [ $\text{gs}^{-1}$ ]	327.5	61.1
Subchannel mass flux [ $\text{kg}(\text{m}^2\text{s})^{-1}$ ]	3759	657.2

Table 2.5: Core conditions applied in simulations of reactivity initiated accidents. The coolant subchannel pertains to a single fuel rod.

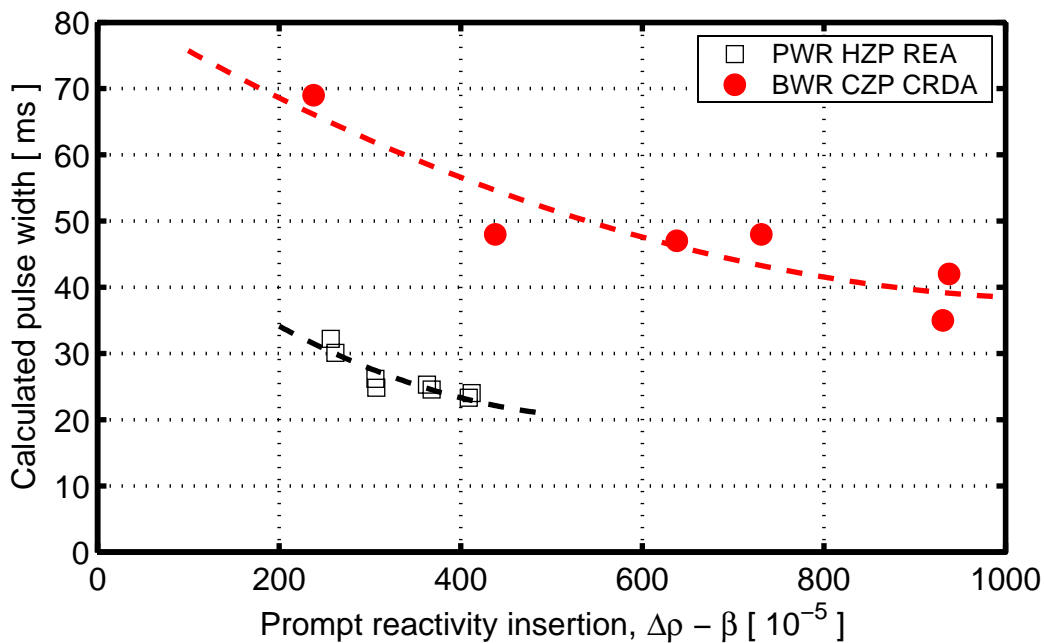


Figure 2.2: Calculated pulse widths. Here,  $\Delta\rho$  is the inserted reactivity, and  $\beta$  is the delayed neutron fraction (In de Betou et al., 2004).

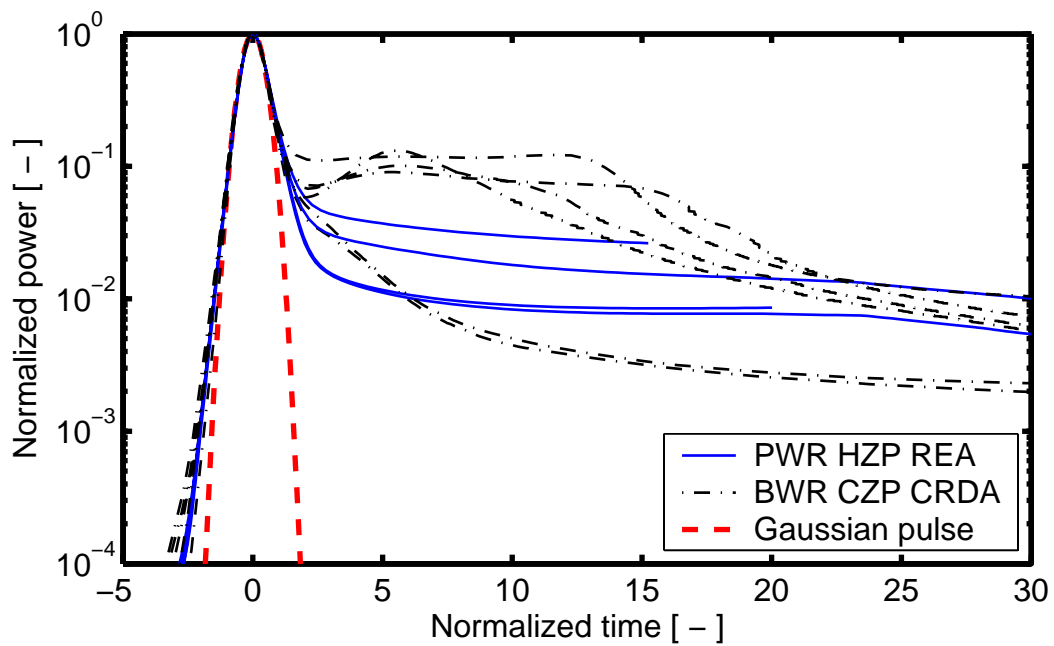


Figure 2.3: Calculated power pulses from three-dimensional core kinetics analyses in comparison with Gaussian pulse. The pulses are normalized (In de Betou et al., 2004).

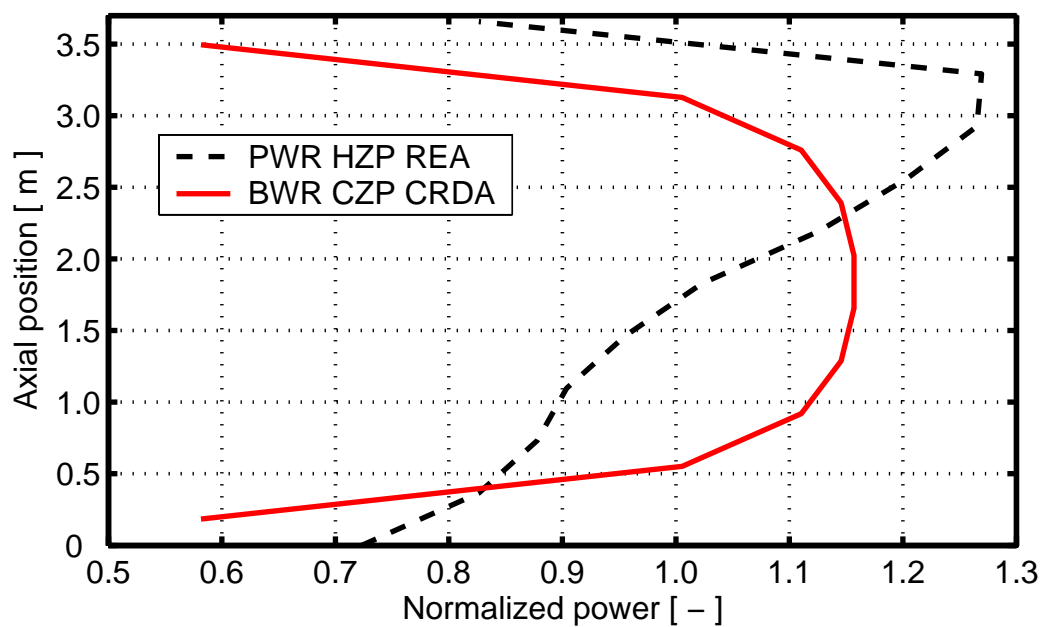


Figure 2.4: Axial power distributions assumed under postulated RIAs.

## 3 Results

Calculated burnup-dependent fuel rod conditions prior to RIA are given in section 3.1. These calculated conditions serve as input to the transient analyses of the actual RIA, the results of which are compiled in section 3.2.

### 3.1 Calculated fuel rod conditions prior to RIA

Key results from the simulated base irradiation of the PWR and BWR fuel rods are summarized in table 3.1. The simulations were performed with the FRAPCON-3.2 computer code, using best-estimate models.

<b>Parameter</b>	<b>PWR rod</b>	<b>BWR rod</b>
Rod average burnup [ MWd(kgU) <sup>-1</sup> ]	70.7	60.6
Rod axial peak burnup [ MWd(kgU) <sup>-1</sup> ]	80.1	70.1
Fission gas release [ % ]	3.72	2.85
Peak clad oxide thickness [ μm ]	74.1	28.6
Peak clad hydrogen content [ wppm ]	555	420

*Table 3.1: Calculated fuel rod properties at end of base irradiation.*

The calculated evolution of clad corrosion and pellet-clad gap conditions are presented in the sequel. These data pertain to the rod axial segment at which clad failure is predicted to occur, i.e. to the axial position of peak power and peak clad corrosion; confer section 2.3.3. For the PWR fuel rod, this is the 9<sup>th</sup> axial segment out of 10, corresponding to an axial elevation of 2.9-3.3 m from bottom of the rod. For the BWR fuel rod, clad failure is predicted to occur in the 6<sup>th</sup> axial segment of the rod, corresponding to an axial elevation of 1.8-2.2 m.

#### 3.1.1 Clad corrosion

Figures 3.1 and 3.2 show the calculated local clad oxide thickness and hydrogen content with respect to local burnup in the peak oxide axial segment of the PWR and BWR fuel rods. The corrosion is calculated by use of best-estimate models for standard Zircaloy-2 and Zircaloy-4 cladding in FRAPCON-3.2 (Berna et al., 1997). In these models, the growth rate of the clad oxide layer is a function of the local fast neutron flux and the metal-oxide interface temperature. The hydrogen content is correlated to the calculated oxide layer thickness, assuming a constant hydrogen pickup fraction, which is set to 0.15 for Zircaloy-4 under PWR conditions, and to 0.29 for Zircaloy-2 under BWR operating conditions. Consequently, the calculated hydrogen content in the clad wall is proportional to the clad oxide layer thickness.

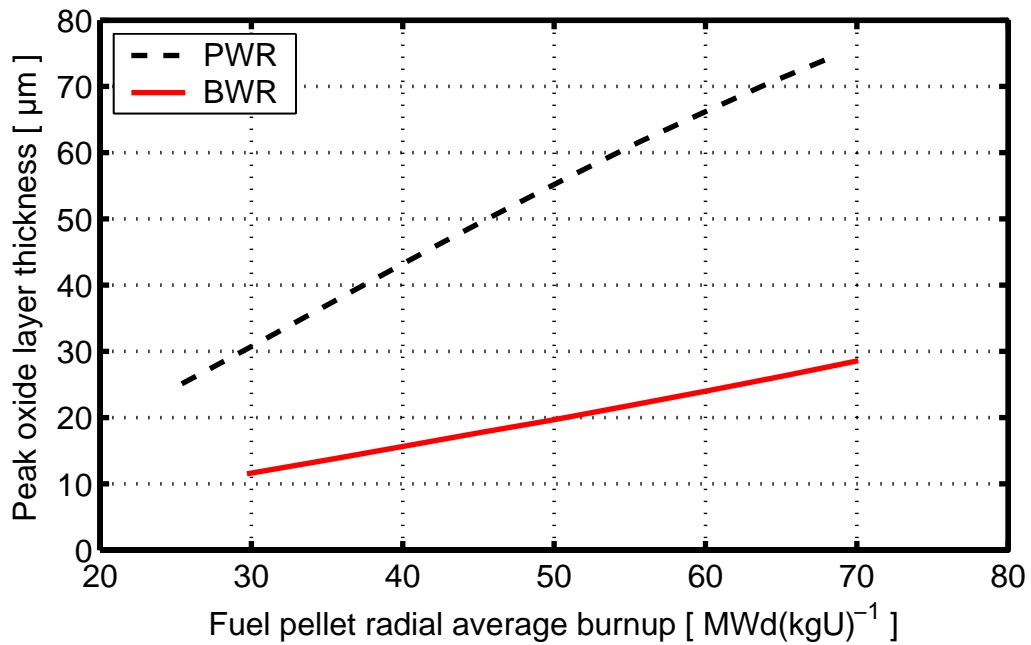


Figure 3.1: Local clad oxide layer thickness with respect to local burnup in the peak oxide axial segment, calculated with best-estimate models in FRAPCON-3.2.

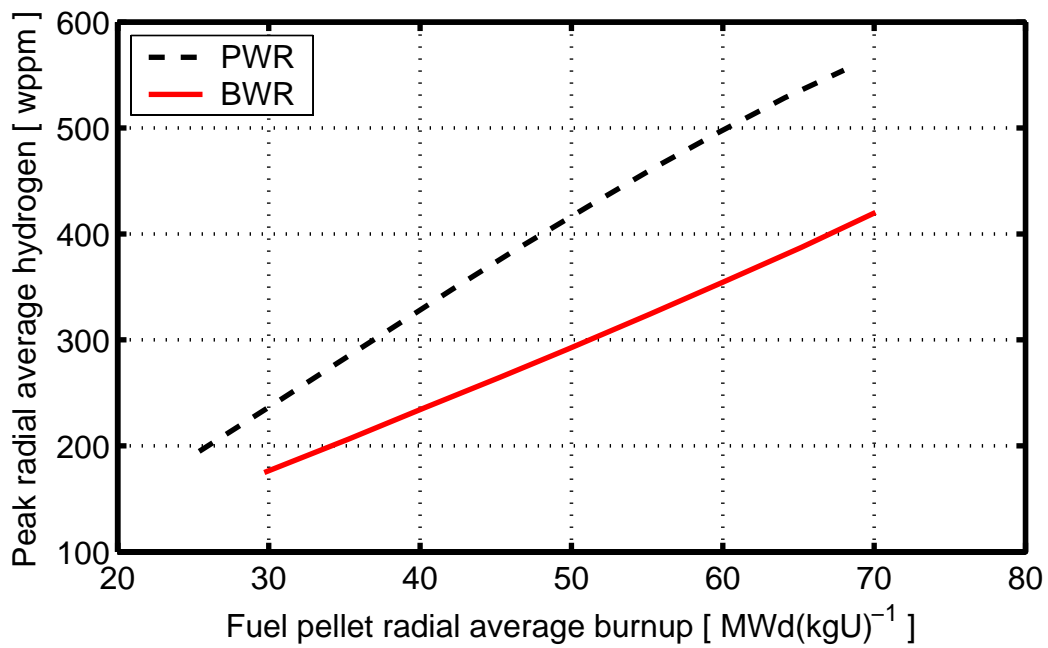


Figure 3.2: Radial average clad hydrogen content with respect to local burnup in the peak oxide axial segment, calculated with best-estimate models in FRAPCON-3.2.

### 3.1.2 Pellet-clad gap conditions

Figures 3.3 and 3.4 show the calculated radial pellet-clad gap size and contact pressure prior to RIA with respect to local burnup in the peak oxide axial segment of the PWR and BWR fuel rod, respectively. Hence, the presented gap conditions are calculated at hot zero power for the PWR rod, and at cold zero power for the BWR rod. Obviously, the pellet-clad gap closes at a burnup of  $38 \text{ MWd}(\text{kgU})^{-1}$  in the PWR fuel rod, whereas it remains open up to  $60 \text{ MWd}(\text{kgU})^{-1}$  in the BWR rod. This is partly due to the difference in clad creep down between PWR and BWR fuel rods, but also the difference in pre-transient coolant pressure (15.5 and 0.1 MPa, respectively) contributes to the disparity in initial gap size.

Figure 3.5 shows the calculated pellet-clad heat transfer coefficient prior to RIA with respect to local burnup in the peak oxide axial segment of the PWR and BWR fuel rods. The heat transfer coefficient is significantly higher for the PWR fuel rod, which is due mainly to the difference in initial gap gas temperature between the PWR and BWR fuel rod. As shown in table 2.5, both the initial coolant temperature and fuel rod power is higher for the PWR fuel rod, which results in higher temperature and improved thermal conductivity for the gas within the pellet-clad gap.

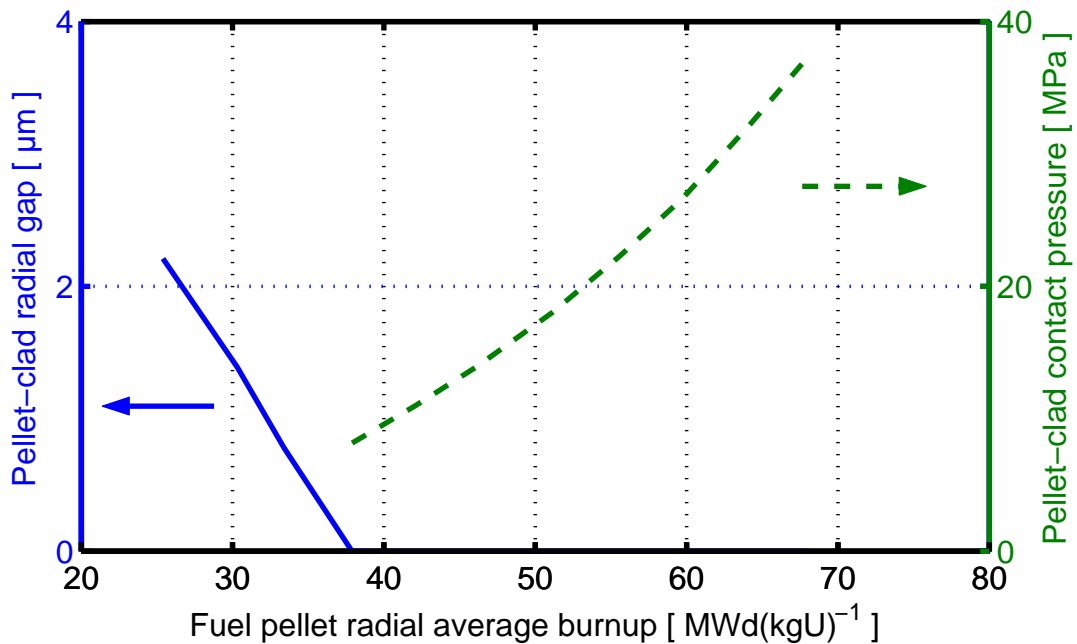


Figure 3.3: Calculated pre-transient pellet-clad radial gap size and contact pressure with respect to local burnup in the peak oxide axial segment of the PWR fuel rod. The gap is calculated at hot zero power, as defined in table 2.5: i.e. for near zero power, coolant pressure of 15.5 MPa and coolant temperature 565 K.

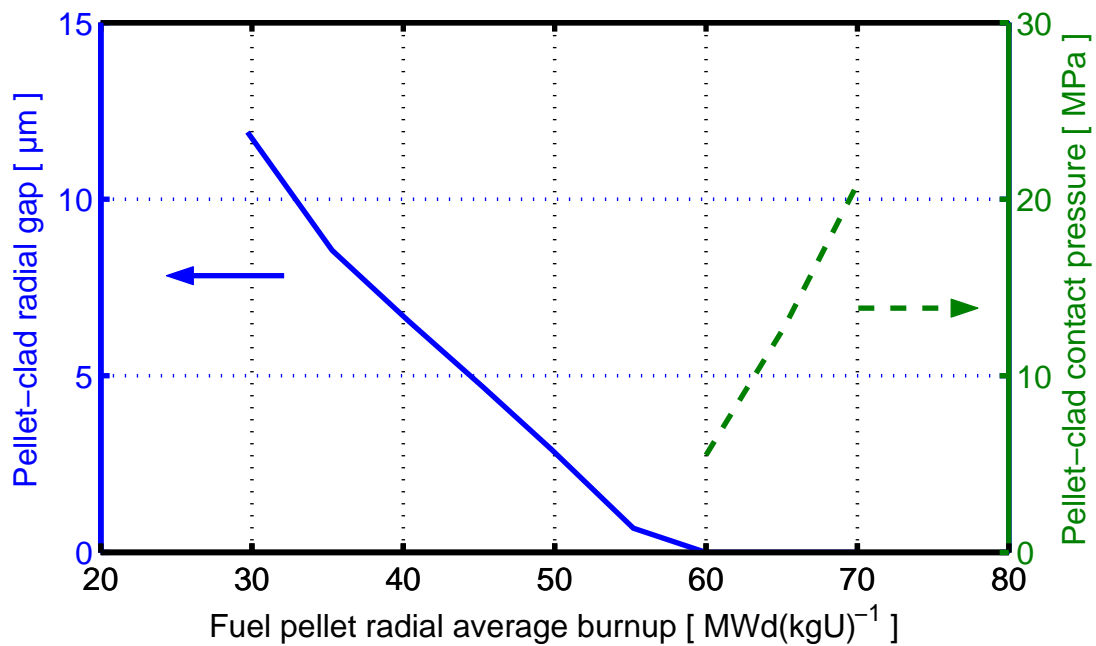


Figure 3.4: Calculated pre-transient pellet-clad radial gap size and contact pressure with respect to local burnup in the peak oxide axial segment of the BWR fuel rod. The gap is calculated at cold zero power conditions, as defined in table 2.5: i.e. for near zero power, coolant pressure of 0.1 MPa and coolant temperature of 303 K.

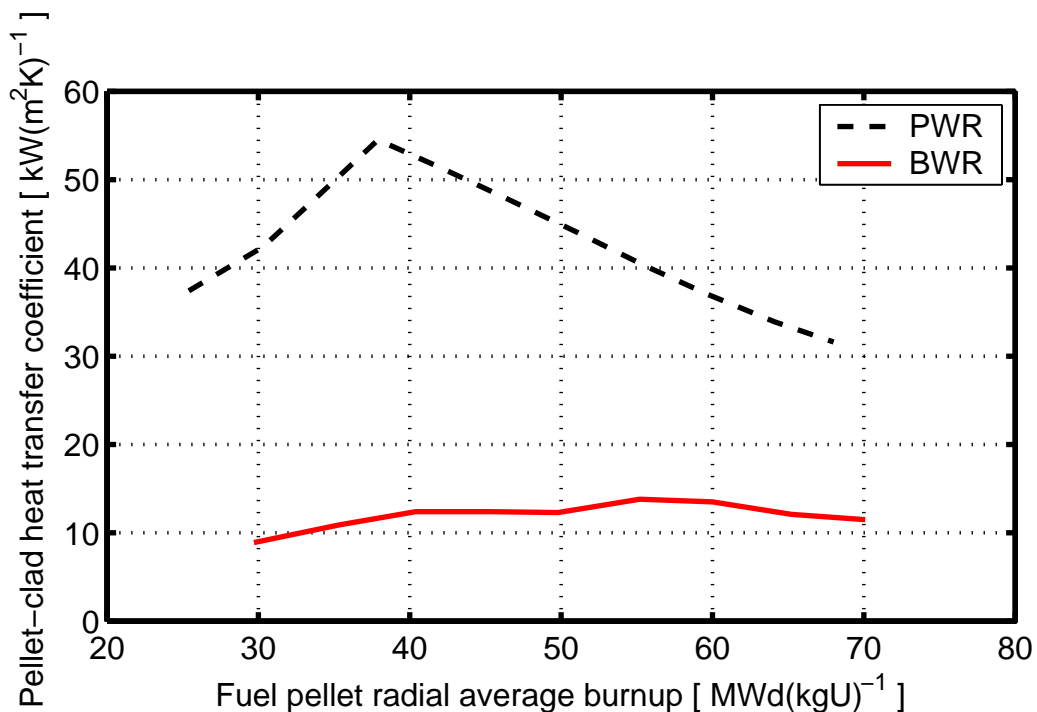


Figure 3.5: Calculated pellet-clad heat transfer coefficient prior to RIA with respect to local burnup in the peak oxide axial segment. The difference between the PWR and BWR rod is caused mainly by differences in gap gas temperature prior to RIA.

### 3.2 Calculated fuel rod conditions under RIA

Key results from the performed analyses of RIA with SCANAIR-3.2 are presented graphically in the sequel. The same data are given in tabular form in appendices C and D. These appendices also contain complementary data, which are not presented in the graphs below. It should be pointed out, that all data pertain to the rod axial segment in which clad failure is predicted to occur, i.e. to the axial position of peak power, peak fuel enthalpy and peak clad corrosion; confer section 2.3.3. For the PWR fuel rod, this is the 9<sup>th</sup> axial segment out of 10, corresponding to an axial elevation of 2.9-3.3 m from bottom of the rod. For the BWR fuel rod, clad failure is predicted to occur in the 6<sup>th</sup> axial segment of the rod, corresponding to an axial elevation of 1.8-2.2 m.

#### 3.2.1 Fuel rod failure thresholds

Figure 3.6 shows the calculated failure thresholds in terms of peak radial average fuel enthalpy under the power pulse, plotted with respect to fuel pellet burnup in the rod axial segment at which clad failure is predicted. Hence, the enthalpy shown in figure 3.6 is *not* the fuel enthalpy at time of failure, but the peak value obtained under a power pulse with sufficient amplitude to just break the cladding. The calculated enthalpy at time of failure is given in appendices C and D for the PWR and BWR event, respectively.

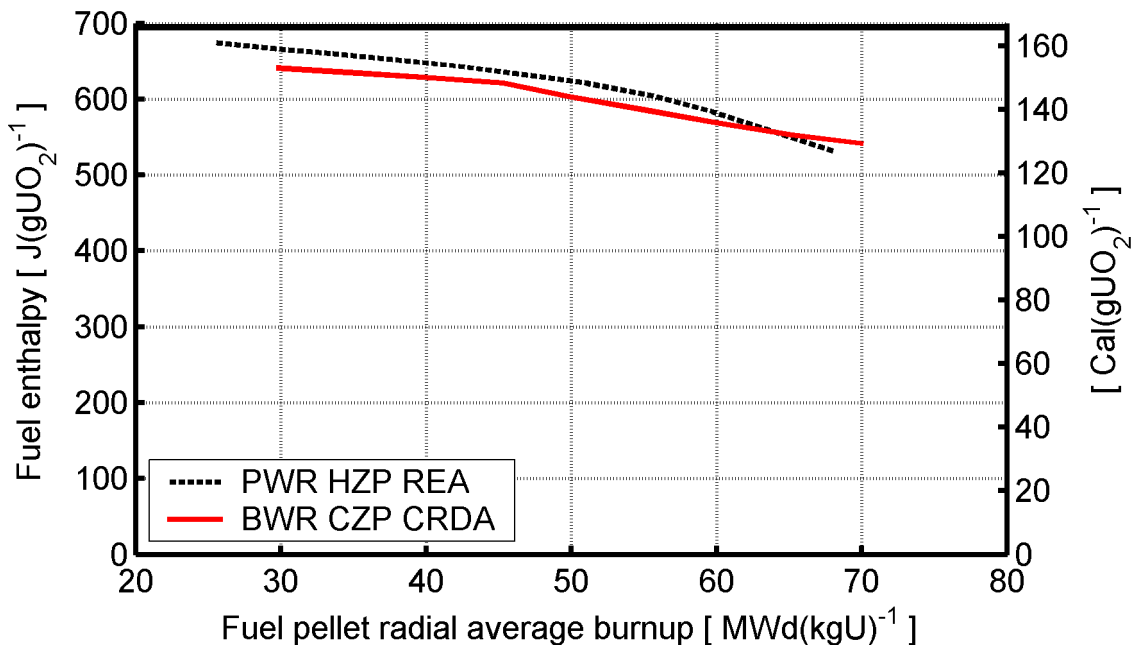


Figure 3.6: Calculated fuel rod failure thresholds for HZP REA and CZP CRDA. The fuel enthalpy is the threshold for fuel rod failure, in terms of peak radial average value during the power pulse.

Figure 3.7 shows basically the same failure thresholds as in figure 3.6, but now with the peak fuel enthalpy *increase* under the postulated RIA on the ordinate. It is generally believed that the fuel enthalpy increase is a more relevant parameter for high-burnup fuel rod failure under an RIA than the total enthalpy, since the enthalpy increase is more directly related to the PCMI-induced loading of the clad tube. The calculated initial fuel enthalpy, prior to the postulated RIA, is  $72.9 \text{ J(gUO}_2\text{)}^{-1}$  for the PWR fuel rod and  $2.6 \text{ J(gUO}_2\text{)}^{-1}$  for the BWR rod. All enthalpies are calculated with respect to a reference temperature of 273 K.

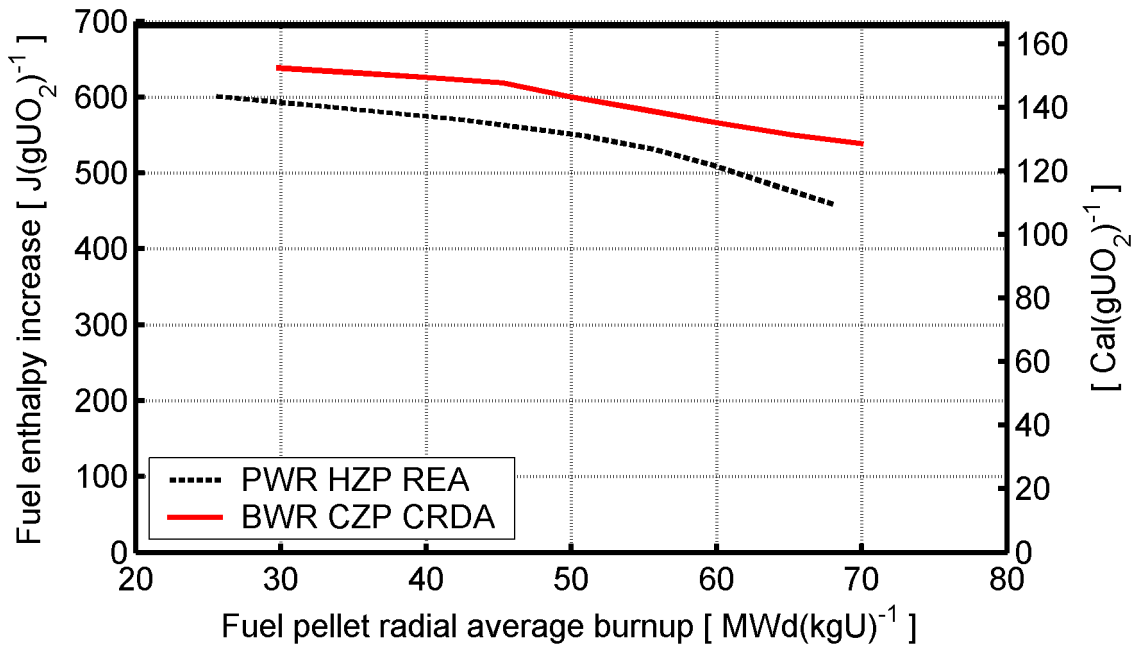


Figure 3.7: Calculated fuel rod failure thresholds for HZP REA and CZP CRDA, in terms of peak fuel enthalpy increase (radial average value).

### 3.2.2 Clad conditions at failure

The calculated clad tube conditions at time of failure are shown in figures 3.8 to 3.10. The strains, strain rates and temperatures in these figures are radial average values, evaluated in the rod axial segment at which clad failure is predicted to occur. The clad stresses at failure are not shown. Since clad tube failure is predicted to take place under plastic deformation, the stresses are dictated by the plastic flow rule and the correlation for clad yield stress applied in SCANAIR-3.2, and do therefore not provide any significant information.

The calculated results in figures 3.6 to 3.10 are thoroughly discussed in section 4.2.

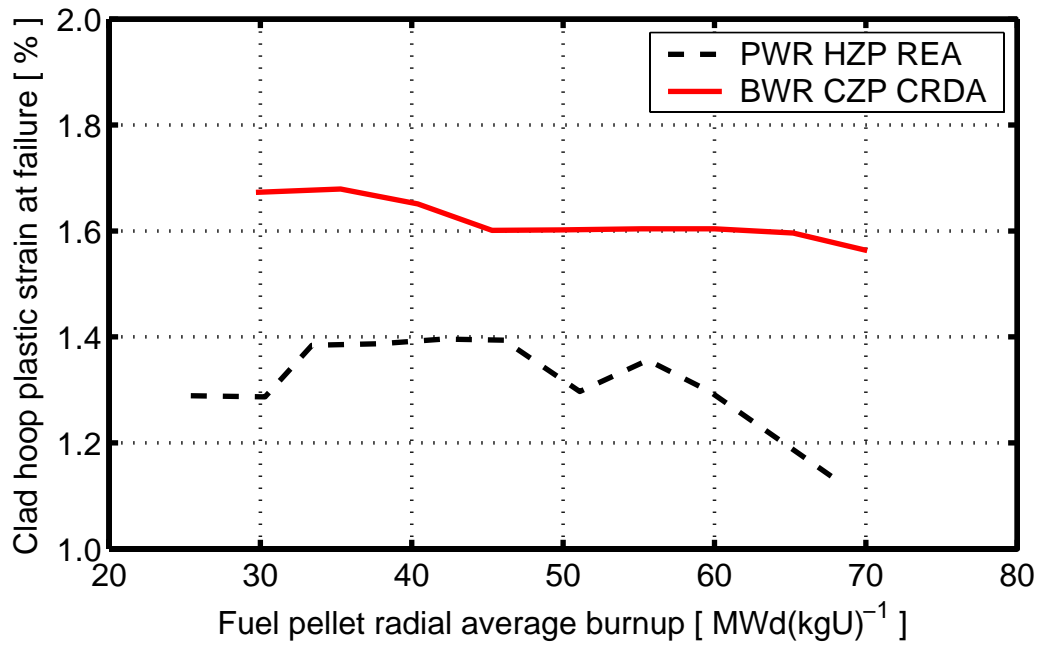


Figure 3.8: Calculated clad hoop plastic strain at failure (radial average value).

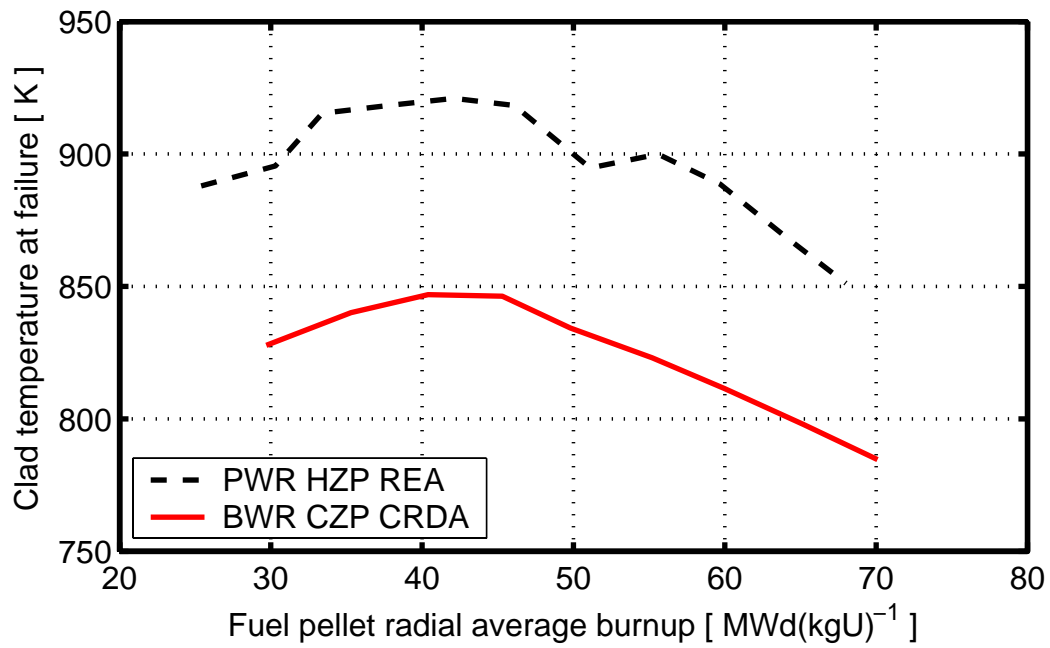


Figure 3.9: Calculated clad temperature at failure (radial average value).

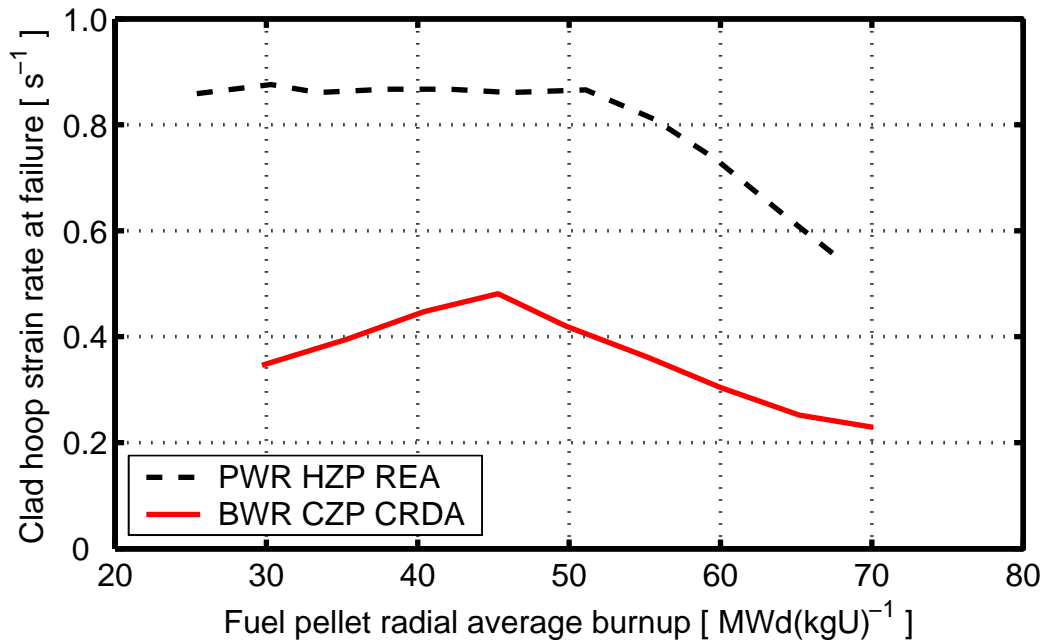


Figure 3.10: Calculated clad hoop strain rate at failure (radial average value).

### 3.2.3 Clad maximum temperature and deformation

Figures 3.11 and 3.12 show maximum hoop plastic strains and temperatures in the clad tube, calculated under threshold conditions, i.e. under the HZP REAs and CZP CRDAs that lead to clad failure. The results are radial average values, evaluated in the rod axial segment at which failure is predicted to occur.

It should be remarked, that these calculated results are fictitious, since SCANAIR-3.2 does not explicitly model the post-failure behaviour of the fuel rod. For instance, leakage of gas through the clad tube breach is not considered, which means that loads from the rod internal gas pressure on the cladding are overestimated under the post-failure part of the transient. Consequently, the maximum hoop plastic strains presented in figure 3.11 should be interpreted as the permanent hoop deformations after RIA, which would be expected if the clad tube actually survived the transient.

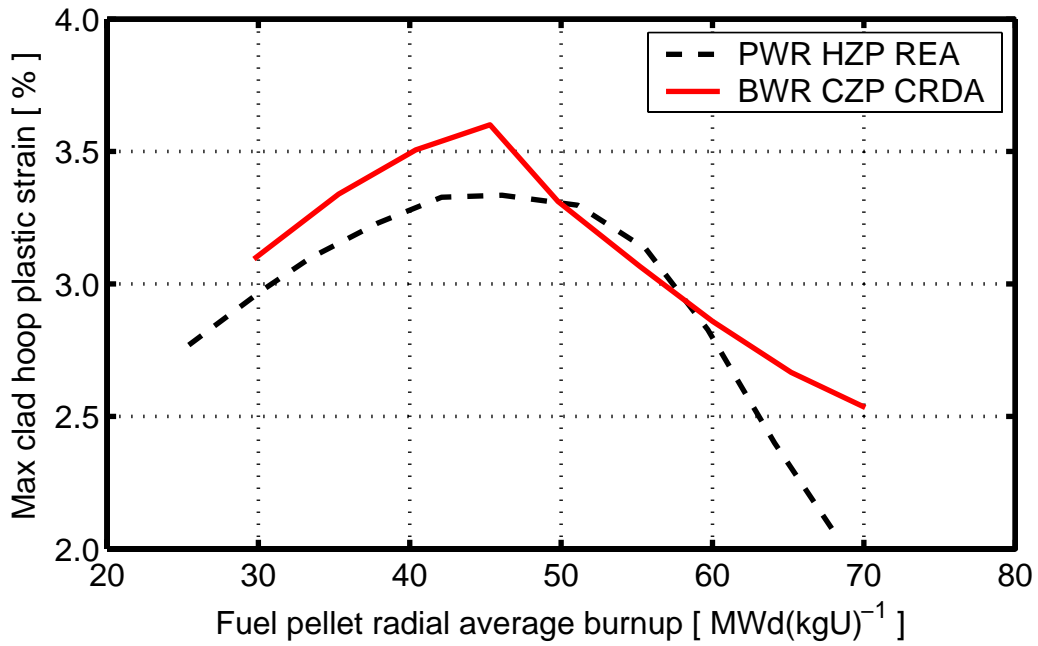


Figure 3.11: Clad maximum hoop plastic strain (radial average value), calculated under threshold conditions.

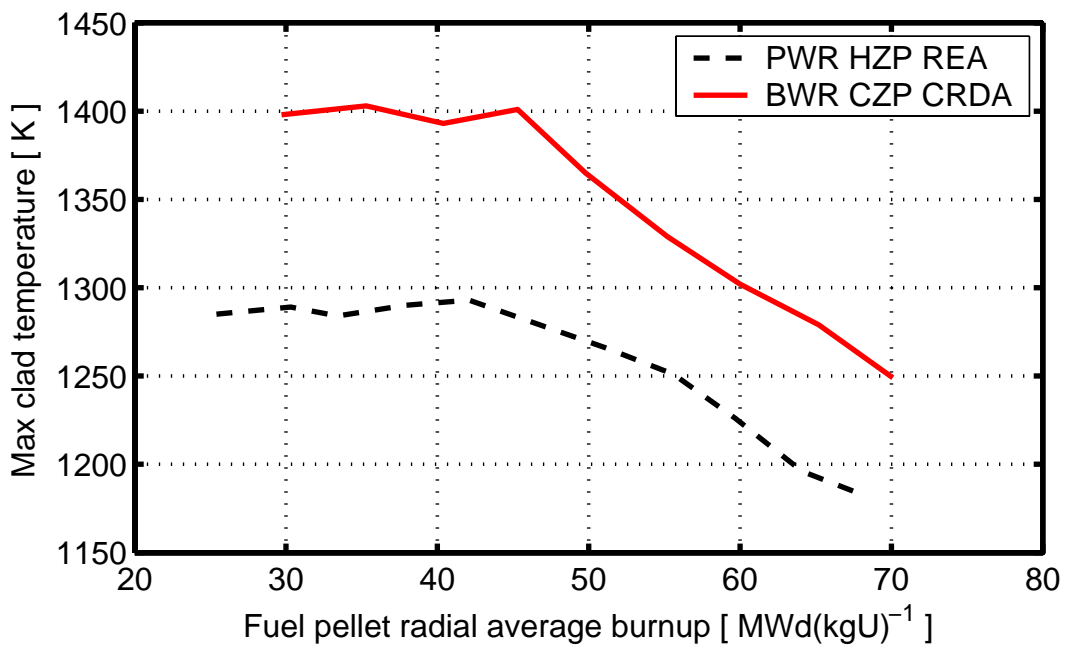


Figure 3.12: Clad maximum temperature (radial average value), calculated under threshold conditions.



## 4 Discussion

The calculated failure thresholds presented in section 3.2.1 should not be viewed as definite operational limits, but merely as best-estimate assessments of the influence of fuel rod burnup on the propensity for PCMI-induced clad tube failure under RIA. The applicability of the calculated failure thresholds is discussed in section 4.1, where also the limitations of the performed analyses are defined. The calculated fuel rod failure thresholds are further evaluated in section 4.2, where comparisons are made with pulse reactor test data and the current fuel rod failure threshold for RIA in Sweden. Comparisons are also made with two other calculated failure thresholds for high-burnup pressurized water reactor fuel, which have recently been presented at international conferences. In order to define operational limits based on the calculated results, one must consider the uncertainties in both input and models applied in analyses. This is discussed in section 4.3, where also the significance of clad corrosion and transient spallation of the clad oxide layer under RIA is investigated by means of parametric sensitivity studies.

### 4.1 Applicability of calculated failure thresholds

Firstly, it should be noticed that the calculated fuel rod failure thresholds in this report are defined with respect to the radial average fuel burnup in the rod axial segment at which clad failure is predicted, and not with respect to the rod *average* burnup. By using local rather than average burnup, comparisons of the calculated failure thresholds with pulse reactor tests on short-length rodlets are made easier. The local burnup in the axial segment at which clad failure occurs,  $E_{loc}$ , is in the performed analyses related to the rod average burnup,  $E_{rod}$ , through

$$E_{loc} = C E_{rod} , \quad (4.1)$$

where the peaking factor  $C$  is 0.961 for the PWR rod, and 1.157 for the BWR rod, respectively.

The failure thresholds in section 3.2.1 are calculated for typical fuel designs, as defined in table 2.3. It should be emphasised, that the failure thresholds are calculated for fuel rods with  $UO_2$  fuel pellets, and that they are not applicable to (U,Pu) $O_2$  mixed oxide (MOX) fuel rods, which at high burnup are known to be more susceptible to failure under RIA than  $UO_2$  fuel rods. The calculated failure thresholds are most likely applicable to burnable absorber (BA) fuel, which usually contains 3-8 wt%  $Gd_2O_3$ . Burnable absorber fuel has a radial power distribution within the pellets, which at low burnup is much different from that in pure  $UO_2$  pellets. However, for the range of burnup covered in our analyses, the difference in radial power distribution is negligible, since the gadolinium is consumed early in life. To our knowledge, no RIA simulation tests in pulse reactors have been performed on BA fuel rods.

The clad tube materials considered in our analyses are standard stress relieved annealed Zircaloy-4 (Zr-1.5Sn-0.2Fe-0.1Cr-0.1O by wt%) for the PWR fuel rod and standard recrystallized Zircaloy-2 (Zr-1.5Sn-0.15Fe-0.1Cr-0.1O by wt%) for the BWR rod. The restriction to these materials is due to the fact that the clad failure criterion applied in analyses is derived from mechanical property tests on Zircaloy-2 and Zircaloy-4 only (Jernkvist et al., 2004). However, the results of our analyses should be applicable also to fuel rods with other clad materials, provided that these materials exhibit ductility and corrosion performance that are equivalent or superior to Zircalloys.

The strain-based clad failure criterion applied in our analyses is strictly focused on PCMI-induced clad tube failure under the early heat-up phase of RIA. Although the results of RIA simulation tests show that this failure mechanism is the most restricting for high-burnup fuel rods, the clad tube may also fail at a later stage of the transient, as a consequence of high temperature and internal gas overpressure. These failures, which result from dry-out or DNB, are relevant to RIAs that initiate from rated power conditions. The high-temperature failure mode is not considered in our study, which pertains to RIAs that initiate from near zero power conditions.

The experimental database behind the failure criterion spans a wide range of cladding conditions, as shown in table 4.1. However, the database does not entirely span the clad tube conditions encountered in our analyses. From figure 3.9, it is evident that calculated clad temperatures at failure are typically 800-900 K, i.e. about 200 K above the temperature interval covered by the database. High-temperature mechanical property tests, preferably conducted under transient heating, are therefore warranted. Uncertainties in the failure criterion and their impact on the calculated fuel rod failure thresholds are discussed in section 4.3.1.

The clad failure criterion applied in our analyses is a best-estimate model, but it should be pointed out that we define fuel rod failure as a loss of clad tube hermeticity, without paying attention to the actual size of the breach. This definition of fuel rod failure is without doubt conservative, but it is judged to be appropriate for evaluations of regulatory acceptance criteria that are focused on retention of radioactive material. Moreover, the failure criterion is based on the assumption that an equal biaxial axial-tangential stress state ( $\sigma_{zz}/\sigma_{\theta\theta}=1$ ) prevails in the clad tube under RIA. This assumption leads to conservative estimates of the clad strain to failure (Jernkvist et al., 2004).

<b>Clad property</b>	<b>Range</b>
Material	Zr-2, Zr-4
Temperature [ K ]	295 – 673
Hoop strain rate [ s <sup>-1</sup> ]	1x10 <sup>-6</sup> – 1.0
Neutron fluence ( $E \geq 1\text{MeV}$ ) [ m <sup>-2</sup> ]	0 – 1.2x10 <sup>26</sup>
Hydrogen content [ wppm ]	0 – 750

*Table 4.1: Range of application for the applied failure criterion. All numbers refer to clad radial average values (Jernkvist et al., 2004).*

Conservative assumptions are also made regarding the power pulse imposed on the fuel under RIA. Firstly, a Gaussian pulse shape is used in our analyses, which leads to conservative estimates of fuel rod failure enthalpies (Jernkvist, 2004). More precisely, fuel rod failure enthalpies calculated with the Gaussian power pulse are about 5% lower than those calculated with the most restricting realistic pulse shapes obtained from the core kinetics analyses by Gabrielson (2004) and Wiksell (2003). Secondly, the axial power distributions are postulated in a conservative manner, such that the peak power under RIA is concentrated at the axial position of peak clad corrosion, and hence at the weakest part of the clad tube. Thirdly, the applied pulse widths, 25 and 45 ms for PWR and BWR, respectively, correspond to the lower end of the results from the above mentioned core kinetics analyses; see figure 2.2. These conservative assumptions are made in order to account for the uncertainties associated with the power generation in high-burnup fuel under RIA.

## **4.2 Evaluation of calculated fuel rod failure thresholds**

### **4.2.1 Comparison with current fuel rod failure threshold**

The calculated fuel rod failure thresholds for PWR HZP REA and BWR CZP CRDA from section 3.2.1 are in figure 4.1 compared with the current fuel rod failure threshold for RIA in Sweden (SKI, 1995). Obviously, the calculated threshold enthalpies for fuel rod failure from our analyses are significantly higher than the current fuel rod failure threshold for RIA. This is hardly surprising, since the failure threshold specified by SKI is based on conservative rendition of pulse reactor test data, whereas our analyses are performed by use of best-estimate computational models.

The calculated failure thresholds drop moderately with increasing burnup, and notwithstanding the differences in postulated accident scenarios between the PWR HZP REA and the BWR CZP CRDA considered in our analyses, the calculated fuel rod failure thresholds for these two events are similar. This may seem somewhat surprising, since the lower pre-transient clad temperature for the BWR rod is expected to have a detrimental effect on clad ductility. However, this detrimental effect is compensated by three factors that speak in favour of the BWR rod:

Firstly, the wider power pulse in the BWR CZP CRDA results in a lower clad strain rate, as shown in figure 3.10, which has a positive effect on clad ductility. In addition, the wider pulse allows more time for heat-up of the clad tube. This is clearly seen in figure 3.9, which shows that the clad temperatures at time of failure differ by no more than about 50 K between the BWR and the PWR fuel rod. Secondly, the clad corrosion is milder for the BWR than for the PWR fuel rod. Clad corrosion is in our analyses evaluated by use of the default best-estimate models for standard Zircaloy-2 and Zircaloy-4 cladding in FRAPCON-3.2. The fuel rod failure thresholds are calculated for the peak oxide axial position of the fuel rod, and the calculated oxide layer thickness and clad hydrogen content at this position is plotted with respect to local burnup in figures 3.1 and 3.2. From these figures, we may conclude that the clad embrittlement due to corrosion is less pronounced for the BWR fuel rod.

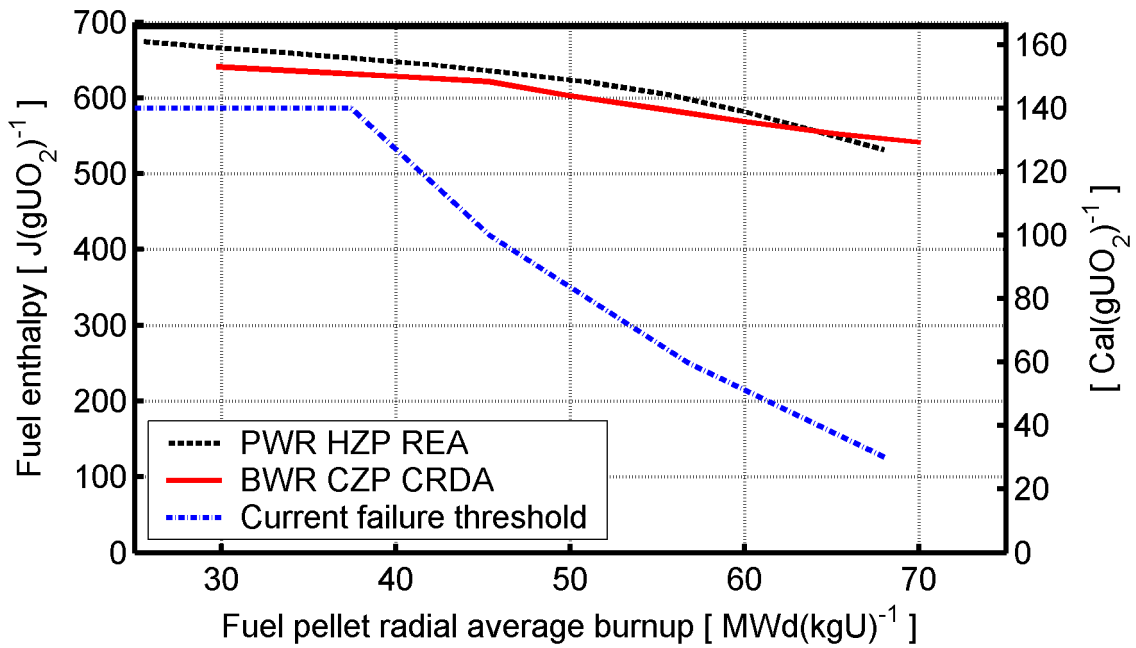


Figure 4.1: Calculated fuel rod failure thresholds, in comparison with the current failure threshold for RIA in Sweden.

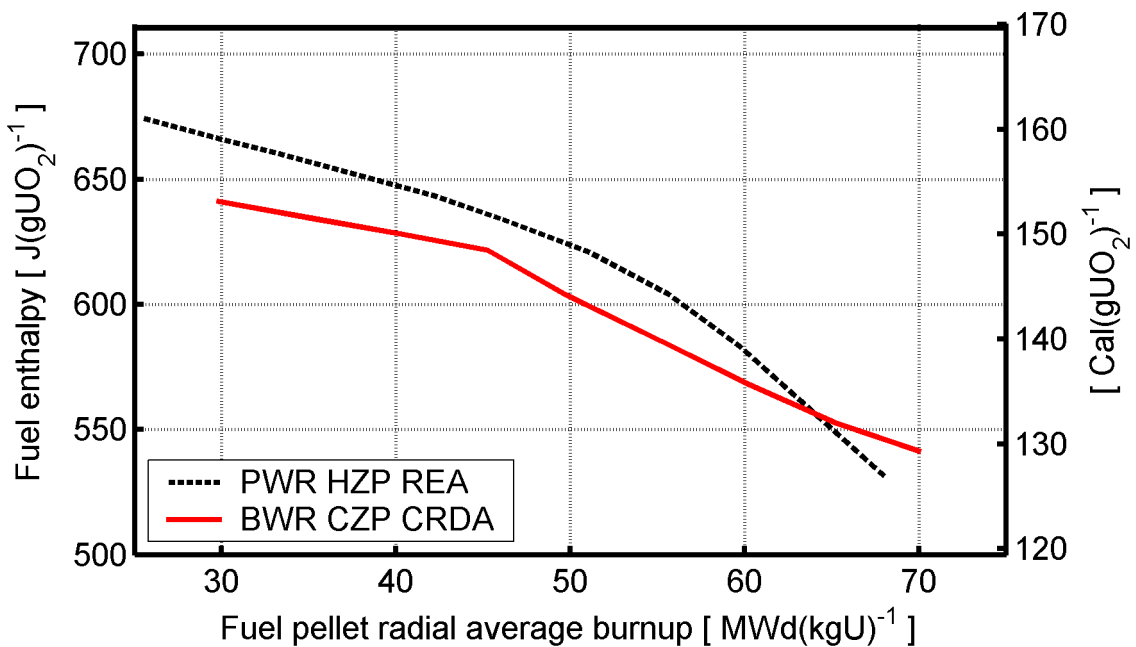


Figure 4.2: Close-up of calculated fuel rod failure thresholds.

In fact, from figure 3.8 we conclude that the lower clad temperature in the BWR fuel rod is actually more than compensated for by the lower strain rate and hydrogen content, since the calculated hoop plastic strain to failure for the BWR rod is slightly higher than for the PWR rod. Thirdly, the differences in pre-transient pellet-clad gap conditions between the BWR and the PWR fuel rod also affect the calculated failure thresholds. As shown in section 3.1.2, the pre-transient pellet-clad mechanical contact state is much milder in the BWR rod. Consequently, for the same degree of pellet expansion under RIA, the PCMI-induced loading on the clad tube will be milder in the BWR than in the PWR fuel rod.

Although the calculated threshold enthalpies are similar for the PWR HZP REA and the BWR CZP CRDA, there are differences in the shape of the failure thresholds. As revealed by the close-up in figure 4.2, the drop in calculated threshold enthalpy with increasing burnup is larger for the PWR event. This is due mainly to the differences in predicted clad corrosion rate between the PWR and BWR fuel rod.

Moreover, the calculated fuel rod failure threshold for the BWR CZP CRDA in figure 4.2 has a nearly bi-linear shape, with a change in slope at a burnup of  $45 \text{ MWd}(\text{kgU})^{-1}$ . This is most likely caused by a change in pellet-clad contact state for the BWR fuel rod at this burnup level. This suspicion is supported by figure 3.10, which reveals a clear peak in calculated clad strain rate at  $45 \text{ MWd}(\text{kgU})^{-1}$ . As shown in figure 3.4, the pre-transient pellet-clad radial gap is approximately  $5 \mu\text{m}$  in the BWR rod at this burnup. The steeper slope of the calculated fuel rod failure threshold above this burnup indicates an aggravated pellet-clad mechanical interaction, caused by the shrinking pellet-clad gap.

The calculated fuel rod failure threshold for the PWR HZP REA in figure 4.2 has a gradual change in slope, and does not show any signs of distinct changes in pellet-clad contact state over the considered range of burnup. From figure 3.3, it is clear that the pre-transient pellet-clad radial gap for the PWR fuel rod is less than  $2 \mu\text{m}$  in our analyses. Hence, if a change in pellet-clad contact state occurs at a pre-transient gap size of  $5 \mu\text{m}$ , as indicated by the results for the BWR fuel rod, this change will not be seen in our calculated failure threshold for the PWR HZP REA.

The calculated evolution of the pre-transient pellet-clad gap conditions with burnup is controlled by the models for pellet fission product swelling and clad creep deformation. The latter model in FRAPCON-3.2 is based on experimental data for Zircaloy-2 materials in BWR environments only (Berna et al., 1997). Still, the model is applied to both BWR and PWR conditions, and no distinction is made between materials with different chemical composition or heat treatment. As reported by Jernkvist and Massih (2002b), the creep model in FRAPCON-3.2 underestimates the creep rate for typical stress-relieved annealed cladding, which is normally used in PWRs. Consequently, it is reasonable to suspect that the calculated pre-transient pellet-clad gap conditions in section 3.1.2 are less accurate for the PWR than for the BWR fuel rod. Moreover, the clad creep model in FRAPCON-3.2 was recently found to be erroneously implemented (Lanning, 2004), and the pre-transient pellet-clad gap conditions in section 3.1.2 were unfortunately calculated before this error was discovered. In clad creep calculations, the fast neutron flux value for the top axial segment of the fuel rod was mistakenly used for every axial segment.

This generally leads to an underprediction of the clad creep rate in the middle part of the rod, where the neutron flux is higher than at the top of the rod. The impact of the underpredicted clad creep rate on the pre-transient pellet-clad gap conditions in section 3.1.2 is two-fold: Firstly, the time (burnup) to gap closure is probably overestimated, which means that the calculated PCMI may be misleadingly mild at low- to intermediate burnup. Likewise, the pellet-clad contact pressure at high burnup is overestimated, which implies that the calculated PCMI would be too severe at high burnup. In summary, the calculated fuel rod failure enthalpies may be somewhat overestimated at low- to moderate burnup, and underestimated at high burnup, as a consequence of the underpredicted clad creep rate.

#### **4.2.2 Comparison with similar studies**

It is interesting to compare our calculated fuel rod failure thresholds with the results of two similar studies, which have recently been reported at international conferences. Both studies have been made in the USA, and they both pertain to PWR rod ejection accidents at hot zero power conditions. However, the computer codes and clad failure criteria used in these two investigations differ, and so do also the modelling approaches. The two studies are briefly summarized below. To our knowledge, no attempts to calculate fuel rod failure thresholds for BWR cold zero power control rod drop accidents have yet been reported in open literature.

##### **4.2.2.1 Study done by EPRI/ANATECH**

The first computational assessment of a fuel rod failure threshold for PWR HZP REA was made by ANATECH, under the auspices of the Electric Power Research Institute (EPRI) in the USA (Yang et al., 2003). All fuel rod analyses were performed with the FALCON computer code, which in contrast to FRAPCON-3.2 is applicable to both steady-state and transient fuel rod analyses. The assumed power transient under the REA was a 20 ms wide Gaussian power pulse, and the threshold enthalpy for fuel rod failure was determined by use of a clad failure criterion based on critical strain energy density (Rashid et al., 2000). This failure criterion was compared with the one used in our analyses in a companion report (Jernkvist et al., 2004).

The failure threshold calculated in the study by EPRI/ANATECH is of conservative nature, since an upper bound corrosion model for low-tin Zircaloy-4 cladding was used in the analyses; see figure 4.3. It should finally be added, that the calculated failure threshold from this study was recently introduced as a regulatory threshold for RIA under PWR and BWR hot reactor conditions by the Swiss Federal Nuclear Safety Inspectorate (Maeder & Wand, 2004).

##### **4.2.2.2 Study done by PNNL**

The Pacific Northwest National Laboratory (PNNL) in the USA has recently presented a fuel rod failure threshold for PWR HZP REA, which is based on calculations with the FRAPCON-3.2 and FRAPTRAN computer codes (Geelhood et al., 2004).

Similar to our analyses, FRAPCON-3.2 was used to generate the burnup-dependent fuel rod initial conditions to the RIA. The considered fuel was of Westinghouse standard 17□17 design, and the simulated base irradiation was representative for a 24-month cycle length. The postulated rod average LHGR was  $27.2 \text{ kWm}^{-1}$  for the first 676 effective full power days, followed by a linear decrease in power with time, ending at  $15.1 \text{ kWm}^{-1}$  after 1235 days of operation. This power history is more challenging than the one used in our analyses; confer figure B.1 in appendix B. This is also reflected in the calculated growth of the clad oxide layer thickness, as shown in figure 4.3. Considering that the same best-estimate corrosion model in FRAPCON-3.2 was used in our analyses and the study by PNNL, the power history applied by PNNL clearly results in faster clad corrosion.

The fuel rod behaviour under REA was analysed with a slightly modified version of FRAPTRAN-1.1 (Cunningham et al., 2001). Among other things, the code was equipped with a strain-based clad failure criterion, intended for prediction of PCMI-induced failures under RIA (Geelhood et al., 2004). The assumed power transient was a 20 ms wide triangular power pulse, i.e. a pulse with constant ramp rate and zero hold time at maximum power. This pulse shape is obviously not realistic, and it yields a lower rate of power increase than a Gaussian pulse of similar width at half maximum.

#### 4.2.2.3 Comparison of calculated results

Figure 4.3 shows a comparison of clad oxide layer thickness as a function of burnup, as applied in the analyses of HZP REA by us, EPRI and PNNL, respectively. As will be further discussed in section 4.3.2, the degree of clad corrosion is important to the fuel rod survivability under RIA, and the differences in clad corrosion revealed by figure 4.3 therefore affect the shape of the calculated fuel rod failure thresholds.

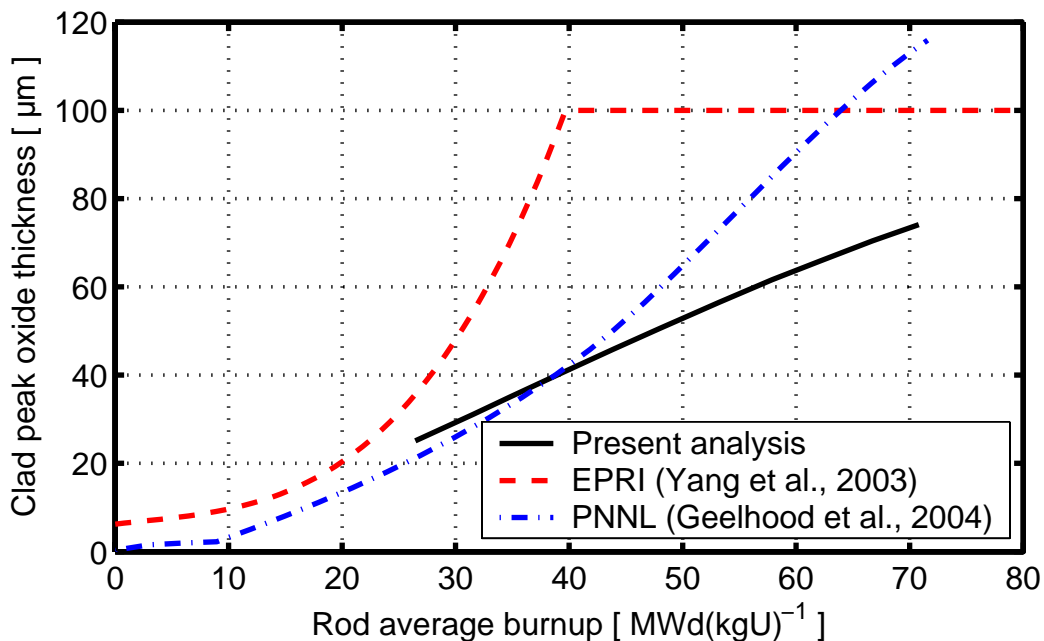


Figure 4.3: Clad peak oxide layer thickness vs. burnup, applied in calculations of fuel rod failure thresholds for PWR HZP REA.

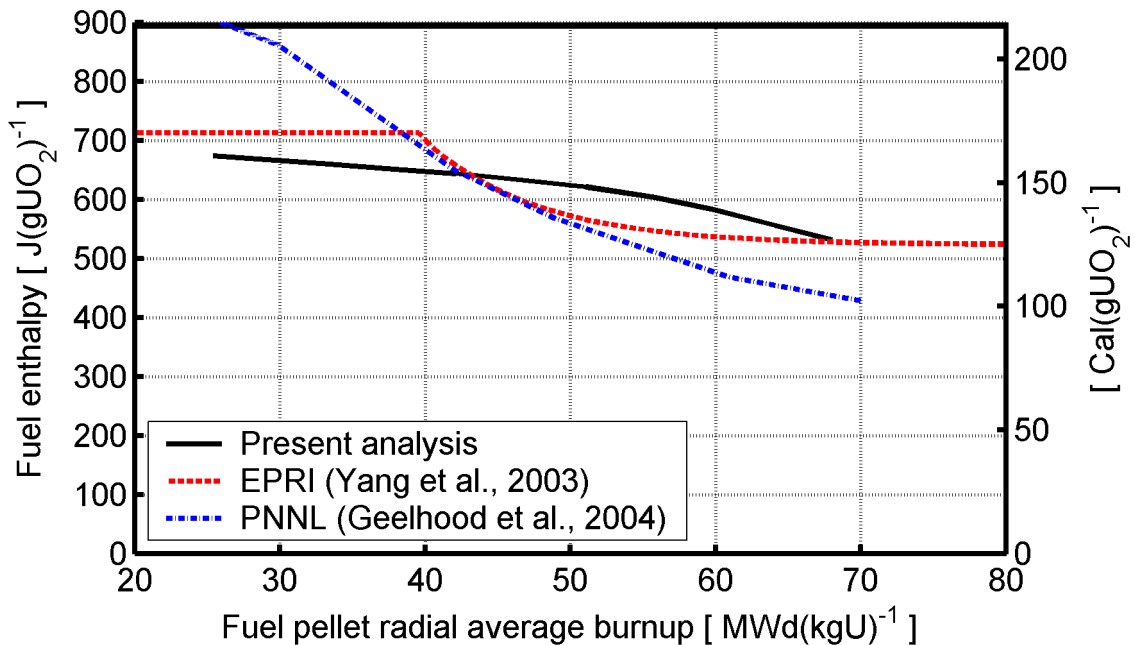


Figure 4.4: Comparison of calculated fuel rod failure thresholds for PWR HZP REA.

The calculated fuel rod failure threshold from our analyses of HZP REA is in figure 4.4 compared with the failure thresholds put forth EPRI and PNNL. It is interesting to note that these calculated failure thresholds are not too far apart, although the trends with respect to fuel burnup are different for the three cases. According to our analyses, the calculated enthalpy threshold decreases almost linearly with fuel burnup up to about 55 MWd(kgU)<sup>-1</sup>, after which the enthalpy threshold falls off with a steeper slope. This is a consequence of our failure criterion, in which the clad ductility is assumed to drop considerably as a result of oxide spallation and non-uniform hydride precipitation as soon as the uniform clad oxide layer thickness exceeds 60 μm (Jernkvist et al., 2004).

The failure threshold by EPRI, on the other hand, shows a nearly constant failure enthalpy for burnups above 55 MWd(kgU)<sup>-1</sup>. This behaviour is caused by the upper bound corrosion model, which makes the clad ductility degradation saturate at a rod average burnup of 40 MWd(kgU)<sup>-1</sup>; confer figure 4.3. At higher burnups, the clad oxide layer is assumed to be 100 μm thick, uniform, and without spallation. Here, it must be questioned why the failure threshold proposed by EPRI tends to a constant value for burnups exceeding 65 MWd(kgU)<sup>-1</sup>. This trend implies that the propensity for fuel rod failure is unaffected by operation further beyond this exposure, which seems unlikely.

The failure threshold calculated by PNNL shows a continuous decrease of the failure enthalpy with fuel burnup. Above 55 MWd(kgU)<sup>-1</sup>, the slope of the curve is similar to that found in our analyses, but large differences exist between these two curves for low- and intermediate burnups. Since FRAPCON-3.2 was used both by us and PNNL for calculating burnup related changes to the fuel rod conditions, the disparate burnup dependence of the calculated failure thresholds must be caused by differences between FRAPTRAN and SCANAIR, and in particular, between the clad failure criteria applied in these codes.

Finally, it should be remarked that the failure enthalpies indicated by the calculated failure threshold by PNNL in figure 4.4 are unrealistically high at low burnup. Fuel rod failures are known to occur at lower enthalpies, as a consequence of departure from nucleate boiling (DNB) and high cladding temperatures. However, this failure mode was not considered in the analyses, either by PNNL or by us.

### 4.2.3 Comparison with pulse test data

The calculated fuel rod failure thresholds from section 3.2.1 are compared with data from 74 RIA simulation tests on pre-irradiated fuel rods from four different pulse reactors in figure 4.5. Open symbols represent fuel rods that survived the tests, whereas filled symbols are failed rods. For details on these tests, the reader is referred to Jernkvist et al. (2004). Obviously, most pulse reactor tests on high-burnup fuel rods fall below the calculated failure thresholds. Failed rods and survivals are interspersed in the diagram, which is due to the fact that large differences exist between the tested rods (fuel design, clad corrosion) as well as between the pulse reactor test facilities (power pulse width, cooling conditions).

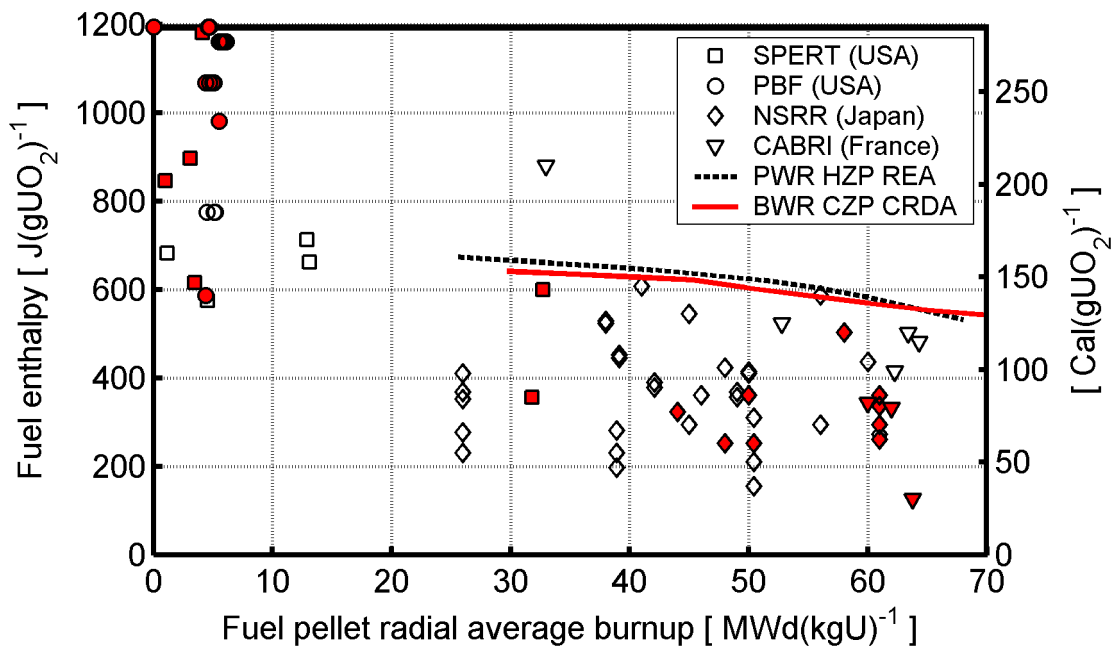


*Figure 4.5: Calculated fuel rod failure thresholds in comparison with pulse test data. The data pertain to radial average peak fuel enthalpy vs. burnup for pre-irradiated uranium dioxide fuel rods, tested in four different pulse reactor facilities. Filled symbols represent failed rods, whereas open symbols are survivals.*

### 4.3 Sensitivity studies

Uncertainties exist in the best-estimate failure criterion applied in our analyses, which affect the calculated results. The uncertainty related to the applied failure criterion can fairly easily be estimated by statistical evaluations of the best-estimate correlation for hoop plastic failure strain and its supporting database. The impact of uncertainty in clad failure prediction on the calculated fuel rod failure threshold is studied in subsection 4.3.1 below.

The calculated results depend on uncertainties in other models as well, and also on the assumptions made about both the postulated RIA and the preceding base irradiation. These uncertainties are more difficult to quantify, but several parametric sensitivity studies were performed in an attempt to estimate the uncertainties in calculated results, and also to identify key parameters and models in the analyses. The impact of applied power pulse shape, pulse width and clad-to-coolant heat transfer models on the calculated fuel rod failure thresholds was studied in a companion report by Jernkvist (2004). In subsections 4.3.2 and 4.3.3 below, the significance of clad corrosion and transient spallation of the clad oxide layer under RIA is analysed by means of simple parametric studies.

#### 4.3.1 Impact of uncertainty in clad failure prediction

The uncertainty related to the strain-based clad failure criterion was statistically evaluated by Jernkvist et al. (2004). More precisely, the relative difference between calculated ( $\varepsilon^c$ ) and measured ( $\varepsilon^m$ ) hoop plastic strain to failure, here defined through

$$\delta\varepsilon = 2 \frac{\varepsilon^c - \varepsilon^m}{\varepsilon^c + \varepsilon^m}, \quad (4.2)$$

was found to have a standard deviation ( $\sigma$ ) of 0.57. Setting  $\delta\varepsilon$  in eq. (4.2) equal to  $\pm 1\sigma$ , we may thus derive a  $\pm 1\sigma$  uncertainty band for the calculated hoop plastic strain to failure

$$\varepsilon^c = \frac{2 \pm \sigma}{2 \mp \sigma} \varepsilon^m. \quad (4.3)$$

With  $\sigma=0.57$  inserted into eq. (4.3), the ratio on the right hand side becomes 1.802 or 0.555, depending on the sign.

Finally, by scaling the calculated clad failure strain from our best-estimate failure criterion with these factors, we obtain a  $\pm 1\sigma$  uncertainty band for the clad hoop plastic strain to failure. With the clad failure strain set to these  $\pm 1\sigma$  uncertainty limits, the fuel rod failure threshold for the postulated PWR HZP REA was re-calculated. The results are shown in figure 4.6, together with the best-estimate failure threshold from section 3.2.1. The  $\pm 1\sigma$  uncertainty band in clad failure strain corresponds roughly to  $\pm 100 \text{ J(gUO}_2\text{)}^{-1}$  in fuel failure enthalpy. This is a surprisingly small variation in enthalpy, considering that the clad hoop plastic strain to failure varies by a factor 1.802/0.555.

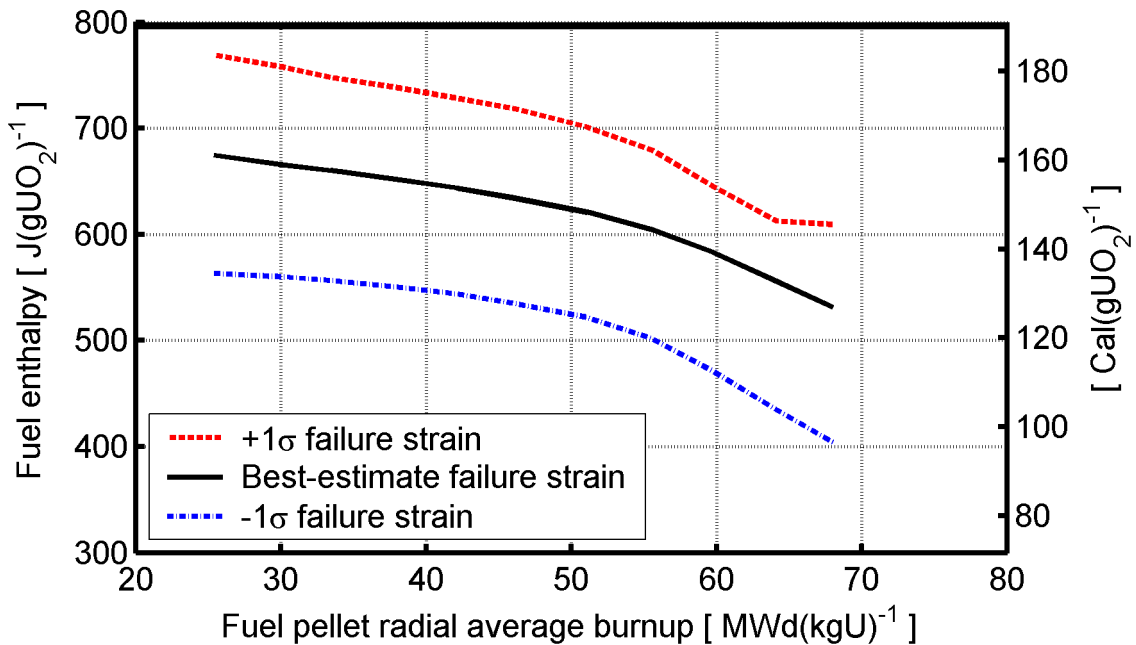


Figure 4.6: Impact of  $\pm 1\sigma$  uncertainty in clad failure strain prediction on calculated fuel rod failure threshold for PWR HZP REA.

#### 4.3.2 Impact of clad corrosion

The impact of clad corrosion is studied by re-calculating the fuel rod failure thresholds, assuming a modified clad oxide layer thickness and hydrogen content. More precisely, we assume a  $\pm 50\%$  variation in the oxide thickness and hydrogen content predicted by the standard best-estimate models in FRAPCON-3.2. The variation is imposed by scaling the calculated best-estimate oxide layer thicknesses in figure 3.1 and the clad hydrogen contents in figure 3.2 by  $\pm 50\%$  in input to SCANAIR. Hence, the analyses with FRAPCON-3.2 are *not* repeated with modified corrosion models, which means that thermal effects of the modified oxide layer thicknesses on the pre-RIA fuel rod conditions, such as altered cladding creep or fuel fission gas release, are neglected.

The impact of the  $\pm 50\%$  variation in clad corrosion on the calculated fuel rod failure threshold is shown in figure 4.7 for the considered PWR HZP REA and in figure 4.8 for the BWR CZP CRDA. Obviously, the variation has a dramatic effect on the calculated failure threshold for the PWR fuel rod, whereas the effect is moderate for the BWR rod. The marked reduction in calculated threshold enthalpy with increasing clad corrosion for the PWR fuel rod is a consequence of our failure criterion, in which the clad ductility is assumed to drop considerably as a result of oxide spallation and non-uniform hydride precipitation as soon as the uniform clad oxide layer thickness exceeds 60  $\mu\text{m}$ . Based on results from mechanical property tests made on clad tubes with spalled oxide, the postulated threshold hoop plastic strain to failure in our criterion is gradually reduced as the oxide layer grows from 60 to 100  $\mu\text{m}$  and spallation degrades the clad ductility through non-uniform hydride precipitation (Jernkvist et al., 2004).

From figure 4.7, we find that the calculated failure enthalpy for PWR fuel rods with fully developed oxide spallation is approximately  $350 \text{ J}(\text{gUO}_2)^{-1}$  at a burnup of  $65 \text{ MWd}(\text{kgU})^{-1}$ . It is worthwhile to compare this result with two RIA simulation tests, performed on PWR fuel rods with spalled cladding oxide in the CABRI pulse reactor (Papin et al., 2002). The results of these tests, REP-Na8 and REP-Na10, are compared with calculated results from our analysis of the PWR fuel rod with nominal +50% corrosion in table 4.2. Obviously, the calculated enthalpy at time of clad failure is in very close agreement with the experimental results.

The calculated clad oxide thickness for the BWR fuel rod is well below  $60 \mu\text{m}$ , as shown in figure 3.1. According to the assumptions made in our failure criterion, no significant detrimental effect of increased corrosion should be expected in this case. As evidenced by figure 4.8, the calculated effect is actually beneficial, since a thicker oxide layer leads to elevated clad temperatures and thereby to larger thermal expansion of the clad tube and in some cases also to slightly improved ductility of the material. The calculated impact of clad oxide thickness on clad temperature and hoop plastic strain at failure is presented in appendix E. As long as the clad oxide layer is uniform, i.e. without spallation, the beneficial effect of increased clad temperature seems to outweigh the detrimental corrosion effects on clad ductility from wall-thinning and increasing hydrogen content. However, this observation is probably an artefact, resulting from the simplistic assumption made in SCANAIR-3.2 that the clad oxide layer remains adherent to the clad tube throughout the transient. This is further discussed in section 4.3.3 below.

It has been suggested by the staff at the United States Nuclear Regulatory Commission (US NRC) that the propensity for fuel rod failure under an RIA is more affected by clad corrosion than by the fuel burnup as such, and that the fuel rod failure threshold for this reason should be defined with respect to clad oxide thickness rather than fuel burnup (Meyer et al., 1997). This suggestion is to some part in line with the results of our study, which indicates that clad corrosion becomes far more important than fuel burnup, once the oxide layer starts to spall. However, as long as the clad oxide layer and hydride distribution are uniform, fuel burnup seems to be the appropriate abscissa to use in definitions of the fuel rod failure threshold. This conclusion is supported by figure 4.9, which shows the same data as in figure 4.7, but plotted in terms of calculated allowable fuel enthalpy increase with respect to clad peak oxide layer thickness.

<b>Parameter</b>	<b>Test REP-Na8</b>	<b>Test REP-Na10</b>	<b>Present calculation</b>
Clad material	Zircaloy-4	Zircaloy-4	Zircaloy-4
Fuel burnup [ $\text{MWd}(\text{kgU})^{-1}$ ]	60	62	64
Power pulse width [ ms ]	75	31	25
Clad oxide thickness (spalled) [ $\mu\text{m}$ ]	130	80	105
Clad hydrogen content [ wppm ]	-	-	793
Peak fuel enthalpy [ $\text{J}(\text{gUO}_2)^{-1}$ ]	443	461	352
Enthalpy at time of failure [ $\text{J}(\text{gUO}_2)^{-1}$ ]	343	331	343

*Table 4.2: Calculated results in comparison with the CABRI REP-Na8 and REP-Na10 pulse reactor tests. The calculations, as well as the tests, pertain to PWR fuel rods with fully developed oxide spallation.*

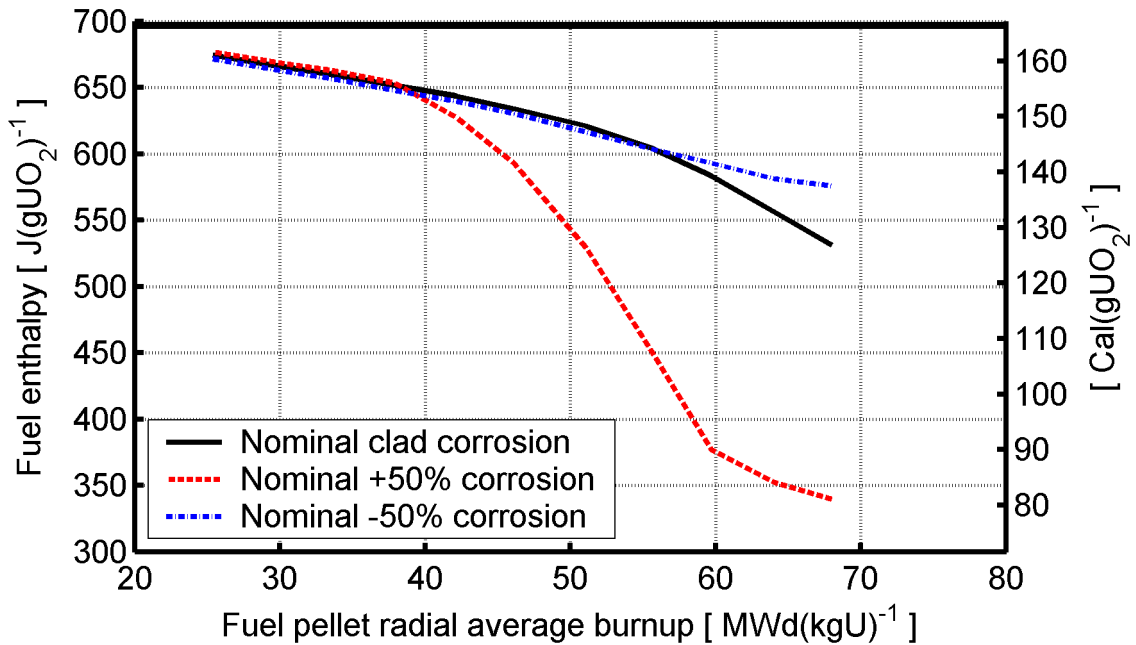


Figure 4.7: Calculated influence of Zircaloy-4 clad corrosion on the fuel failure threshold for PWR HZP REA. Nominal corrosion refers to standard best-estimate models in FRAPCON-3.2; confer figures 3.1 and 3.2.

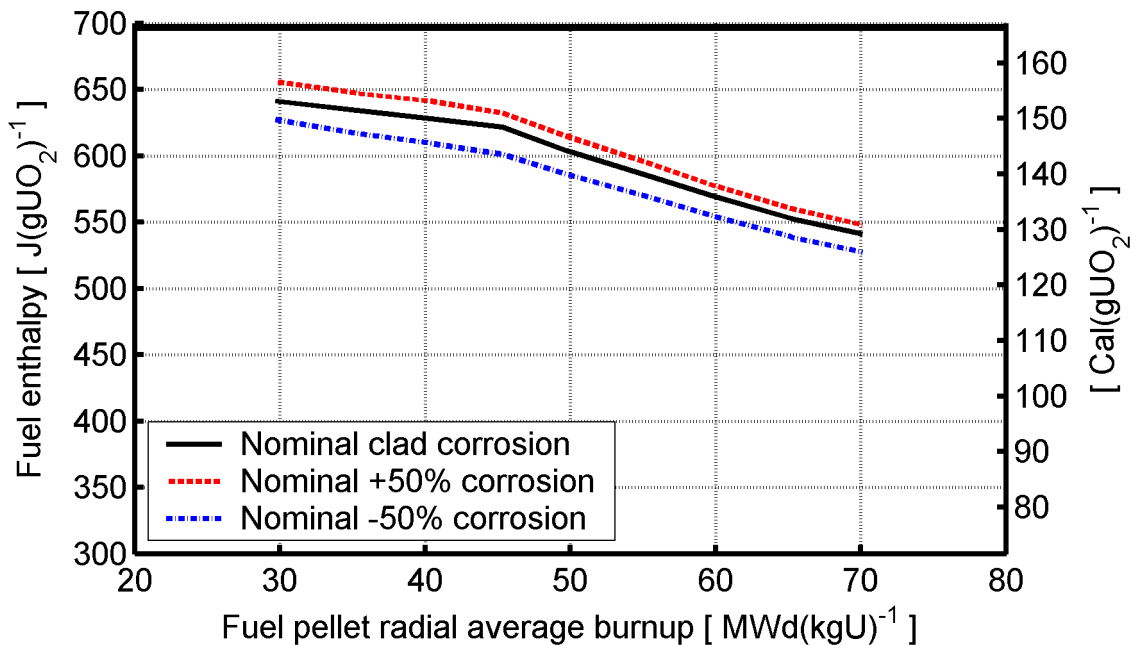


Figure 4.8: Calculated influence of Zircaloy-2 clad corrosion on the fuel failure threshold for BWR CZP CRDA. Nominal corrosion refers to standard best-estimate models in FRAPCON-3.2; confer figures 3.1 and 3.2.

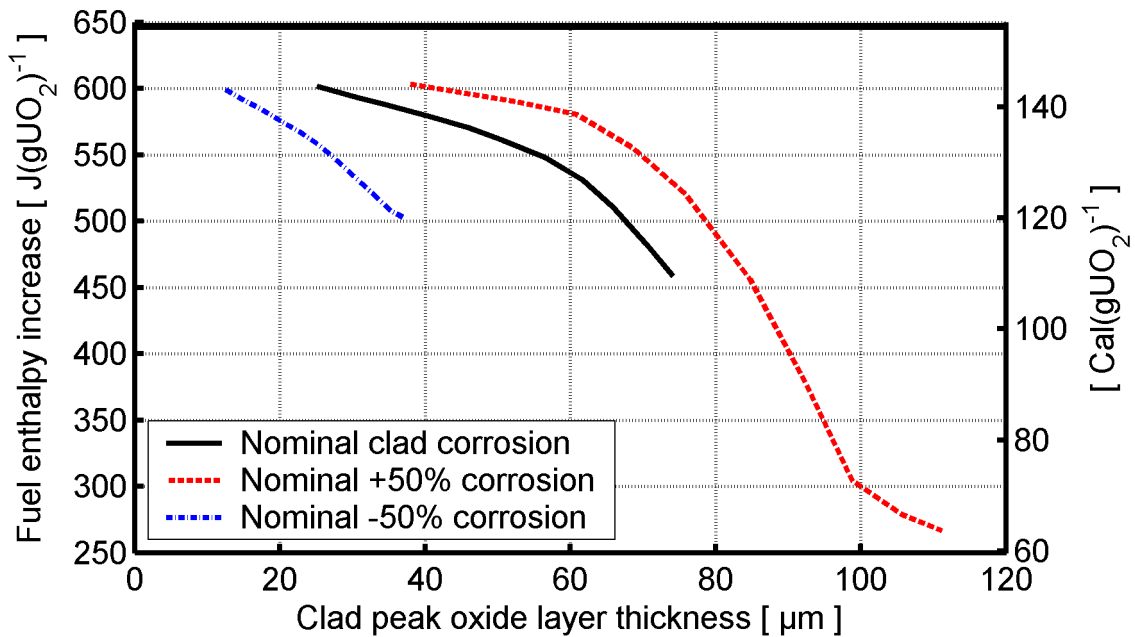


Figure 4.9: Calculated failure thresholds for PWR HZP REA. The allowable fuel enthalpy increase under the REA is plotted with respect to peak clad oxide thickness.

If clad corrosion were the controlling parameter for fuel rod survivability under RIA, we would expect the three curves in figure 4.9 to coincide. However, the curves differ significantly, which indicates that other burnup related parameters, such as the pellet-clad gap conditions, are more important to the rod survivability than the clad oxide thickness, provided the clad corrosion is moderate. Consequently, as long as the oxide layer is non-spalled and possible hydrides in the clad material are uniformly distributed, clad corrosion is of minor importance to the calculated fuel rod failure thresholds, as illustrated in figures 4.7 and 4.8.

#### 4.3.3 Impact of clad oxide spallation under RIA

The conclusion drawn in the foregoing section that a thick uniform oxide layer may have a beneficial effect on clad survivability under an RIA is doubtful. The weak beneficial effect observed in our analyses is due to the low thermal conductivity of the oxide layer, approximately  $2 \text{ W(mK)}^{-1}$ , which leads to a rise in clad temperature as the oxide layer thickens. The temperature rise results in larger thermal expansion of the clad tube, and in some cases also to a slightly improved clad ductility as the oxide layer thickens. This insulating effect may be of importance if the oxide layer remains adherent to the clad tube surface throughout the transient. However, pulse reactor tests performed on severely corroded PWR fuel rods have shown that thick oxide layers are prone to spall under RIA conditions (Schmitz & Papin, 1999).

The influence of oxide spallation under RIA on clad-to-coolant heat transfer has not yet been studied experimentally, let alone modelled in computer codes (Bessiron, 2004). However, one may assume that the oxide layer remains adherent to the clad surface until a critical stress or strain for delamination is attained at the oxide-metal interface. Up to the time of spallation, the oxide layer acts not only as a barrier for radial heat flow, but also as a heat sink. The heated oxide then spalls off, the metal cladding gets into direct contact with the coolant, and a new oxide film starts to form.

The impact of transiently spalling oxide on the clad-to-coolant heat transfer under RIA is here qualitatively assessed by a rather hypothetical calculation, in which the thermal conductivity and heat capacity of the oxide layer are altered so that lowest possible clad temperatures are obtained under the considered RIA. Consequently, the thermal conductivity of the oxide layer is set to infinity ( $1000 \text{ W(mK)}^{-1}$  in analyses with SCANAIR), thereby entirely eliminating its insulating effect throughout the entire RIA. Hence, the time-dependence of the spallation process is neglected. The heat capacity of the oxide is on the other hand retained at its nominal value, which means that the oxide layer still acts as heat sink. This apparently inconsistent manipulation of thermal properties for the clad oxide layer results in lowest possible clad temperatures under RIA, as calculated with SCANAIR.

Re-calculated fuel rod failure thresholds with modified oxide thermal conductivity (“spalling oxide”) are compared with the original failure thresholds from section 3.2.1 (“adherent oxide”) in figures 4.10 and 4.11. According to our calculations, transient spallation of the clad oxide layer under RIA may lead to a reduction of the fuel rod failure enthalpy by at most 10 to 30  $\text{J(gUO}_2\text{)}^{-1}$ . This fairly moderate reduction is due to improved clad-to-coolant heat transfer, which results in lower clad temperature, thermal expansion and ductility: the calculated impact of oxide spallation on clad temperature and hoop plastic strain at failure is presented in appendix F.

It is interesting to note that the calculated reduction of failure enthalpy in the transiently spalled fuel rods seems almost independent of burnup, and thus also independent of the clad oxide layer thickness. Moreover, there is a noticeable difference in calculated enthalpy reduction between the PWR and BWR event. As revealed by figures 4.10 and 4.11, the calculated impact of oxide spallation under RIA is stronger for the BWR CZP CRDA. This is most likely a result of the wider power pulse, which makes the calculated failure enthalpy more sensitive to perturbations in the clad-to-coolant heat transfer.

Finally, it must be concluded that the beneficial effect of a thick uniform oxide layer on clad survivability under RIA, which was observed in section 4.3.2, would probably not appear if transient spallation of the clad oxide layer under RIA were satisfactory modelled in SCANAIR.

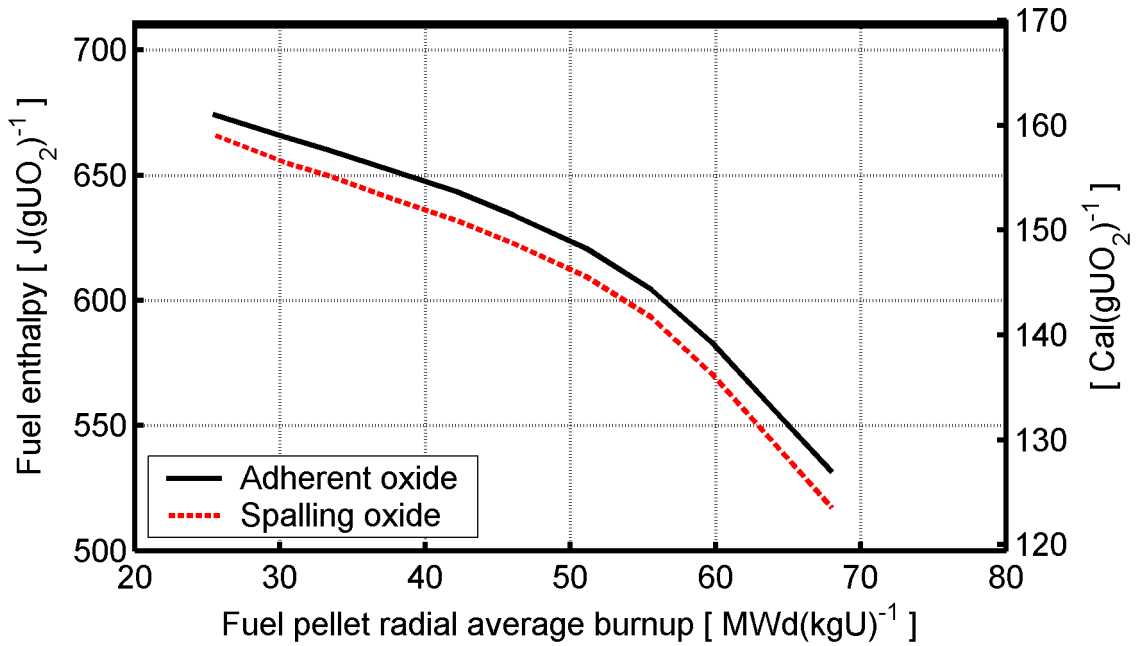


Figure 4.10: Calculated impact of transiently spalling clad oxide on the fuel failure threshold for PWR HZP REA. The case with adherent oxide refers to the calculated best-estimate failure threshold in figure 3.6.

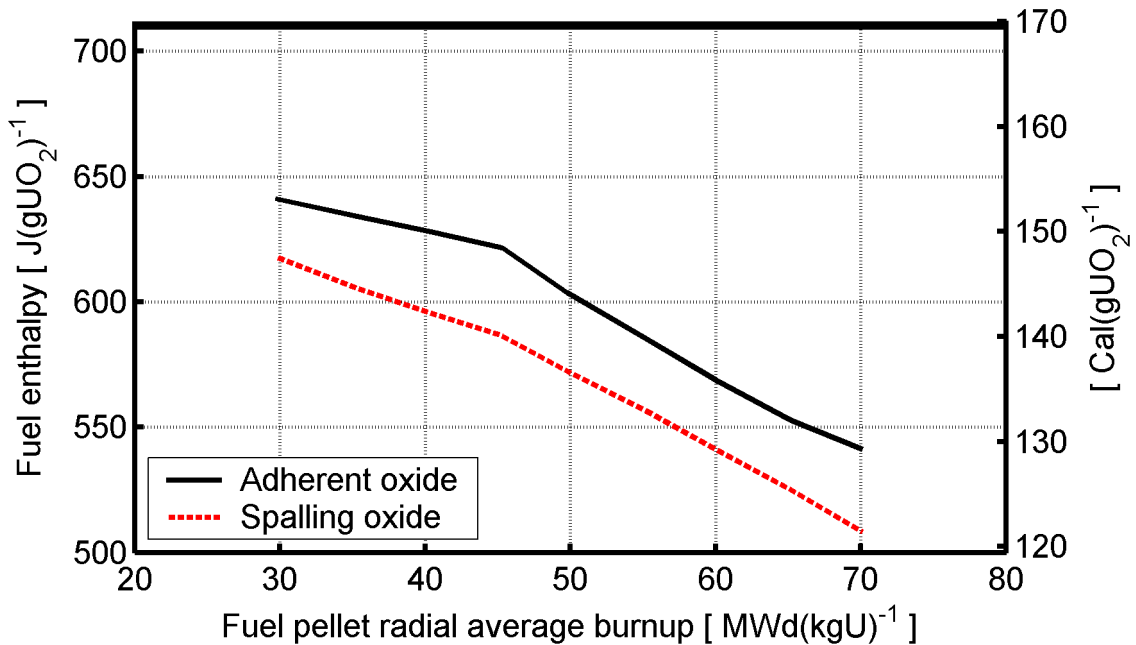


Figure 4.11: Calculated impact of transiently spalling clad oxide on the fuel failure threshold for BWR CZP CRDA. The case with adherent oxide refers to the calculated best-estimate failure threshold in figure 3.6.

## 5 Conclusions

Burnup-dependent failure thresholds for high-burnup light water reactor UO<sub>2</sub> fuel rods subjected to postulated RIAs were assessed by use of best-estimate computational methods. The considered accident scenarios were the PWR HZP REA and the BWR CZP CRDA. The power excursions under these postulated events were in analyses represented by a Gaussian power pulse, with a fixed width of either 25 ms (HZP REA) or 45 ms (CZP CRDA). These applied power pulses were based on a conservative evaluation of results from three-dimensional core kinetics analyses.

Failure thresholds for HZP REA and CZP CRDA, formulated in terms of allowable fuel enthalpy with respect to fuel burnup, were calculated for fuel burnups ranging from 30 to 70 MWd(kgU)<sup>-1</sup> by use of the FRAPCON-3.2 and SCANAIR-3.2 computer codes. Although differences exist in postulated accident scenarios between the HZP REA and the CZP CRDA considered in analyses, the calculated fuel rod failure thresholds for these two events are similar. The calculated failure enthalpy decreases gradually with fuel burnup, from approximately 650 J(gUO<sub>2</sub>)<sup>-1</sup> at 30 MWd(kgU)<sup>-1</sup> to 530 J(gUO<sub>2</sub>)<sup>-1</sup> at 70 MWd(kgU)<sup>-1</sup>. Calculated clad temperatures and hoop plastic strains at time of clad failure are typically 800-900 K and 1.2-1.6 %, respectively, for both the HZP REA and the CZP CRDA. Calculated hoop strain rates at failure are 0.6-0.9 s<sup>-1</sup> for the considered HZP REA and 0.2-0.5 s<sup>-1</sup> for the CZP CRDA.

The calculated fuel rod failure thresholds presented in this report provide best-estimate assessments of the influence of fuel rod burnup on the propensity for PCMI-induced clad tube failure under RIA. However, the calculated results are inevitably affected by uncertainties in the best-estimate models and input data applied in analyses. Parametric sensitivity studies were therefore performed in order to estimate uncertainties in calculated results, and also to identify key parameters and models in the analyses. The impact of postulated power pulse shape and pulse width on the calculated fuel rod failure thresholds was the topic of a companion report (Jernkvist, 2004), in which also the influence of applied models for clad-to-coolant heat transfer was investigated. These sensitivity studies indicated that the pulse width may have a significant impact on the failure enthalpy, at least for pulses narrower than 50 ms.

In the present report, further sensitivity studies were pursued, in order to quantify the impact of clad corrosion and clad oxide spallation on the calculated fuel rod failure thresholds. From these studies, we conclude that clad corrosion has a minor effect on the fuel rod survivability under RIA, as long as the clad oxide layer is non-spalled and possible hydrides in the material are uniformly distributed. However, for cladding tubes with spalled oxide, the ductility of the material may be dramatically reduced as a consequence of non-uniform hydride precipitation, and the failure threshold significantly lower. The calculated failure enthalpy for PWR fuel rods with spalled oxide is approximately 350 J(gUO<sub>2</sub>)<sup>-1</sup> at a fuel burnup of 65 MWd(kgU)<sup>-1</sup>. This result is in very close agreement with two RIA simulation tests, performed on PWR fuel rods with Zircaloy-4 cladding and spalled oxide in the CABRI pulse reactor.

Finally, the calculated best-estimate fuel rod failure threshold for PWR HZP REA was complemented with a sensitivity study, in which the impact of uncertainties related to the applied failure criterion was statistically quantified. The analysis showed that a  $\pm 1\sigma$  uncertainty in predicted clad hoop plastic strain to failure resulted in a  $\pm 100 \text{ J}(\text{gUO}_2)^{-1}$  variation in calculated failure enthalpy for the PWR fuel rod. Here,  $\sigma$  denotes the standard deviation of the relative error in predicted clad hoop plastic strain to failure, which is 0.57 for the failure criterion applied in our analyses.

In conclusion, the performed analyses indicate that a common fuel rod failure threshold for PWR HZP REA and BWR CZP CRDA, expressed in terms of allowable fuel enthalpy with respect to fuel burnup, is feasible, provided that the threshold is applied to fuel rods with non-spalled clad oxide. If the clad oxide layer is spalled, one may suspect that the clad ductility is degraded by non-uniform hydride precipitation. In this case, the fuel rod failure behaviour is controlled by the local clad ductility in spalled regions of the clad tube, whereas the fuel burnup is of minor importance. Consequently, it is probably not meaningful to define a fuel rod failure threshold with respect to fuel burnup, if oxide spallation cannot be ruled out.

## 6 References

- Berna, G.A., Beyer, C.E., Davis, K.L. and Lanning, D.D., 1997.  
*FRAPCON-3: A Computer Code for the Calculation of Steady-State, Thermal-Mechanical Behavior of Oxide Fuel Rods for High Burnup*,  
NUREG Report NUREG/CR-6534, Volume 2 (1997).
- Bessiron, V., 2004.  
*Clad-to-Coolant Heat Transfer during a RIA Transient: Analysis of the PATRICIA Experiments, Modelling and Applications*, Paper presented at the Fuel Safety Research Meeting, Tokyo, Japan, March 1-2, 2004.
- Cunningham, M., Beyer, C.E., Medvedev, P.G. and Berna, G.A., 2001.  
*FRAPTRAN: A Computer Code for the Transient Analysis of Oxide Fuel Rods*,  
NUREG Report NUREG/CR-6739, Volume 1, August 2001.
- Federici, E., Lamare, F., Bessiron, V. and Papin, J., 2000.  
*Status of Development of the SCANAIR Code for the Description of Fuel Behavior under Reactivity Initiated Accidents*, Proc. of the 2000 Int. Topical Meeting on LWR Fuel Performance, Park City, Utah, USA, April 10-13, 2000.
- Gabrielson, P., 2004.  
*Effektpulskarakteristik vid RIA för PWR*, (In Swedish),  
Vattenfall Bränsle Report PB-236/03, January 2004.
- Geelhood, K.J., Beyer, C.E. and Cunningham, M.E., 2004.  
*Modifications to FRAPTRAN to Predict Fuel Rod Failures due to PCMI during RIA-Type Accidents*, Proc. of the 2004 Int. Meeting on LWR Fuel Performance, Orlando, Florida, USA, September 19-22, 2004.
- IAEA, 2001.  
*Thermohydraulic Relationships for Advanced Water Cooled Reactors*,  
Report IAEA-TECDOC-1203, International Atomic Energy Agency, Vienna, Austria.
- In de Betou, J., Jernkvist, L.O., Massih, A.R., Rudling, P., Rönnerberg, G., Stepniewski, M. and Wiksell, G., 2004. *Assessment of Burnup-Dependent Fuel Rod Failure Threshold under Reactivity-Initiated Accidents in Light Water Reactors*, Proc. of the 2004 Int. Meeting on LWR Fuel Performance, Orlando, Florida, USA, September 19-22, 2004.
- Jernkvist, L.O., 2002.  
*FRAPAIR: An Interface Program between FRAPCON-3 and SCANAIR 3.2*,  
Quantum Technologies Report TR 02-003, Uppsala, Sweden.
- Jernkvist, L.O., 2004.  
*Sensitivity Study on Clad Tube Failure under Reactivity Initiated Accidents in Light Water Reactors*, Swedish Nuclear Power Inspectorate (SKI) Research Report 2004:34, Stockholm, Sweden.

- Jernkvist, L.O. and Massih, A.R., 2002a.  
*Analysis of the Effect of UO<sub>2</sub> High Burnup Microstructure on Fission Gas Release*, Swedish Nuclear Power Inspectorate (SKI) Research Report 02:56, Stockholm, Sweden.
- Jernkvist, L.O. and Massih, A.R., 2002b.  
*Evaluation of the FRAPCON-3 Computer Code*, Swedish Nuclear Power Inspectorate (SKI) Research Report 02:29, Stockholm, Sweden.
- Jernkvist, L.O., Massih, A.R. and Rudling, P., 2004.  
*A Strain-Based Clad Failure Criterion for Reactivity Initiated Accidents in Light Water Reactors*, Swedish Nuclear Power Inspectorate (SKI) Research Report 2004:32, Stockholm, Sweden.
- Lanning, D.D., 2004.  
*Low-Impact Error in FRAPCON-3 Creep Calculation*,  
Electronic Mail to the FRAPCON-3 User Group Members, November 11, 2004.  
Pacific Northwest National Laboratory, Richland, Washington, USA.
- Lanning, D.D., Beyer, C.E. and Berna, G.A., 1997.  
*FRAPCON-3: Integral Assessment*,  
NUREG Report NUREG/CR-6534, Volume 3 (1997).
- Maeder, C. and Wand, H., 2004.  
*Sicherheitskriterien für Reaktivitätsstörfälle in Schweizerischen Kernkraftwerken*,  
(In German), Report HSK-AN-5208, Swiss Federal Nuclear Safety Inspectorate (HSK),  
Villigen, Switzerland.
- Manzel, R. and Walker, C.T., 2000.  
*High Burnup Fuel Microstructure and Its Effect on Fuel Rod Performance*,  
Proc. of the 2000 Int. Topical Meeting on LWR Fuel Performance, Park City, Utah,  
USA, April 10-13, 2000.
- Meyer, R.O., McCardell, R.K. and Scott, H.B., 1997.  
*A Regulatory Assessment of Test Data for Reactivity Accidents*,  
Proc. ANS Topical Meeting on Light Water Reactor Fuel Performance, Portland,  
Oregon, March 2-6, 1997, pp 729-744.
- Papin, J., Lemoine, F. and Federici, E., 2002.  
*Main Outcomes from the CABRI Test Results*, Proc. NEA CSNI Topical Meeting on  
RIA Fuel Safety Criteria, Aix-en-Provence, France, May 13-15, 2002.  
Report NEA/CSNI/R(2003)8/Vol 2, pp 61-81.
- Rashid, Y.R., Montgomery, R.O., Lyon, W.F. and Yang, R., 2000.  
*A Cladding Failure Model for Fuel Rods Subjected to Operational and Accident  
Transients*, Proc. of the IAEA Technical Committee Meeting on Nuclear Fuel  
Behaviour Modelling at High Burnup and its Experimental Support, Windermere, UK,  
June 19-23, 2000.

Schmitz, F. and Papin, J., 1999.  
*High Burnup Effects on Fuel Behaviour under Accident Conditions: the Tests CABRI REP-Na*, J. Nucl. Mat. 270, pp 55-64.

SKI, 1995.  
*Ändrade gränser för härd- och kapslingskada vid analys av reaktivitetsolyckor*, (In Swedish), SKI Beslut 5.66-941618, Swedish Nuclear Power Inspectorate (SKI), January 18, 1995.

Wiksell, G., 2003.  
*Pulsbredder vid transienter beräknade med S3K*, (In Swedish), OKG Report 2003-08073.

Yang, R., Montgomery, R.O. and Waeckel, N., 2003.  
*Revised Reactivity Initiated Accident Acceptance Criteria for High Burnup Fuel*, Proc. European Nuclear Society ENS TopFuel 2003 Conference, Wurzburg, Germany, March 16-19, 2003.



## Appendix A: Current fuel rod failure threshold for RIA in Sweden

The current fuel rod failure threshold for reactivity initiated accidents in Sweden was defined by the Swedish Nuclear Power Inspectorate (SKI) in the beginning of 1995 (SKI, 1995). The failure threshold was defined in terms of maximum allowable radial average fuel pellet enthalpy [ $\text{cal}(\text{gUO}_2)^{-1}$ ] with respect to fuel pellet radial average burnup [ $\text{MWd}(\text{kgUO}_2)^{-1}$ ], as shown in the table below. For convenience, the threshold is also transformed to units applied throughout this report. Figure A.1 shows the fuel rod failure threshold, together with the results of 74 RIA simulation tests on pre-irradiated fuel rods from four different pulse reactors. Open symbols represent fuel rods that have survived the tests, whereas filled symbols are failed rods. For details on these tests, the reader is referred to Jernkvist et al. (2004).

Fuel pellet radial average burnup [ $\text{MWd}(\text{kgUO}_2)^{-1}$ ]	Fuel pellet radial average enthalpy [ $\text{cal}(\text{gUO}_2)^{-1}$ ]	Fuel pellet radial average burnup [ $\text{MWd}(\text{kgU})^{-1}$ ],	Fuel pellet radial average burnup [ $\text{J}(\text{gUO}_2)^{-1}$ ]
0	140	0.0	586
33	140	37.4	586
40	100	45.4	419
50	60	56.7	251
60	30	68.0	126

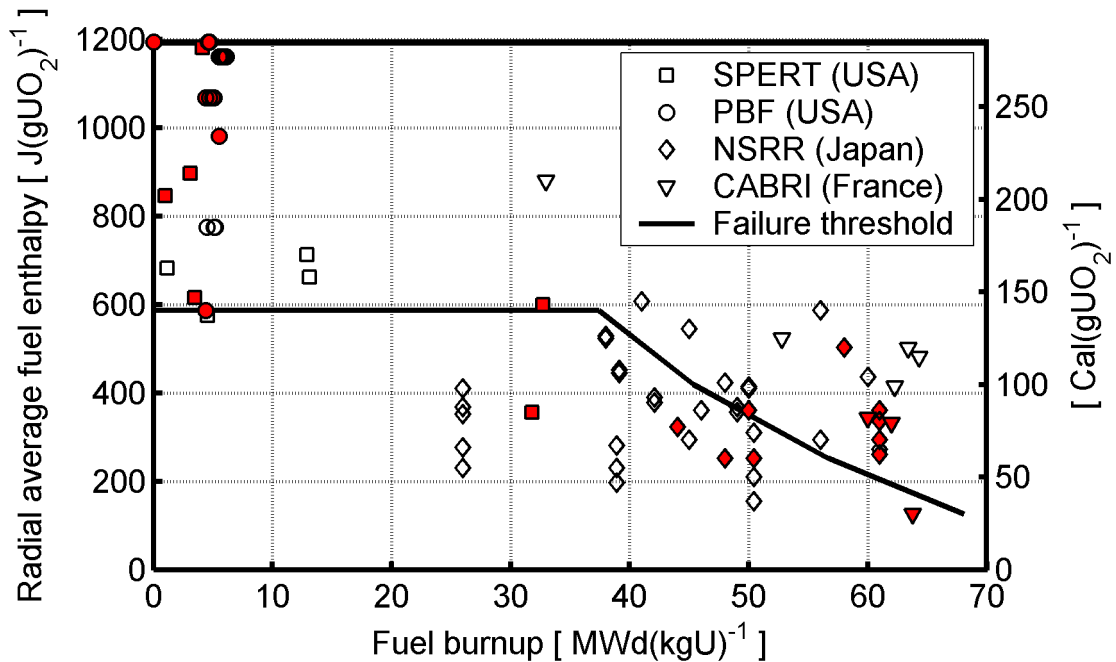


Figure A.1: The current fuel rod failure threshold applied in Sweden, in comparison with pulse test data. The data pertain to radial average peak fuel enthalpy vs. burnup for pre-irradiated uranium dioxide fuel rods, tested in four different pulse reactor facilities. Filled symbols represent failed rods, whereas open symbols are survivals.

## Appendix B: Power histories and axial power distributions applied in simulations of base irradiation

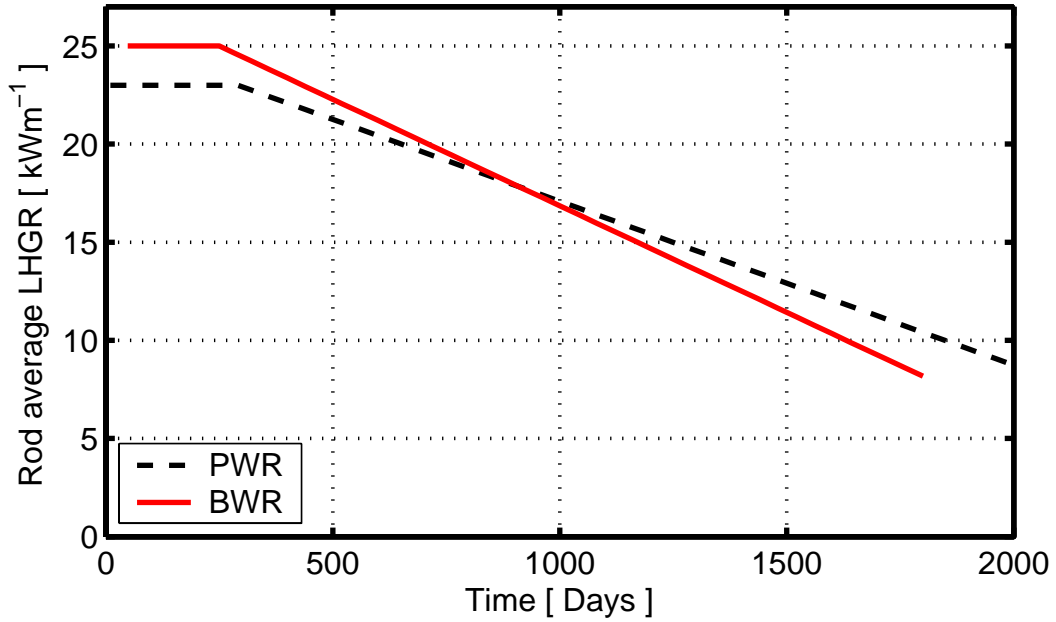


Figure B.1: Steady-state base irradiation histories assumed in analyses.

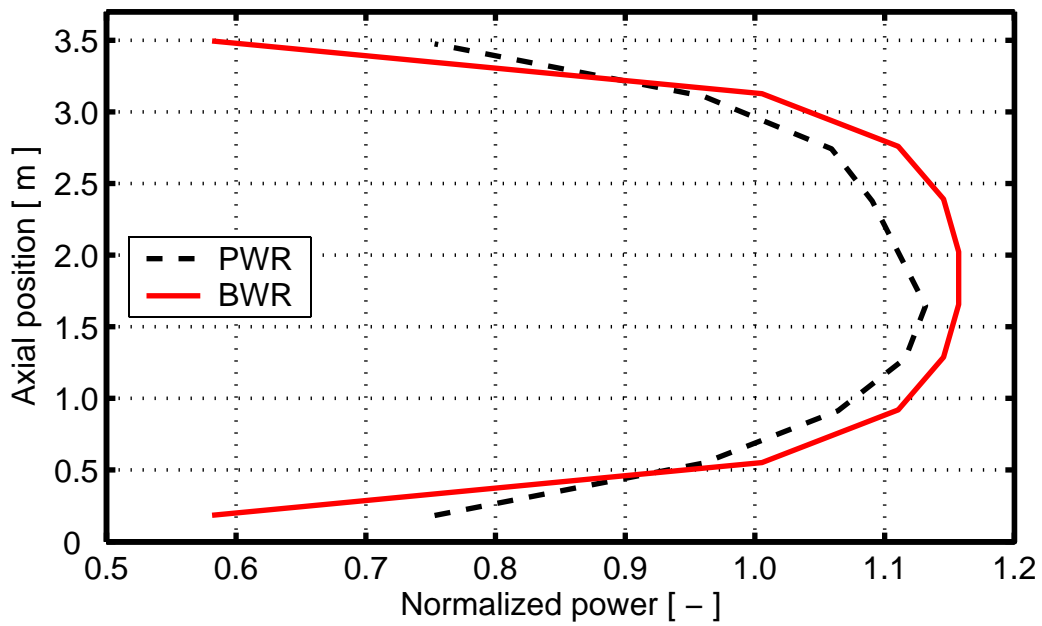


Figure B.2: Axial power distributions applied under steady-state base irradiation.

## Appendix C: Calculated fuel rod failure conditions under PWR HZP REA

Parameter	Fuel local burnup [ MWd(kgU) <sup>-1</sup> ]										
	25.4	30.3	33.4	37.9	42.1	46.1	51.1	55.6	59.7	64.1	68.0
Peak fuel enthalpy [ J(gUO <sub>2</sub> ) <sup>-1</sup> ]	674	665	660	651	644	634	621	604	583	556	531
Time to peak fuel enthalpy [ ms ]	101	101	101	101	101	101	101	101	101	101	101
Fuel enthalpy at clad failure [ J(gUO <sub>2</sub> ) <sup>-1</sup> ]	613	605	600	593	586	578	566	551	532	507	485
Time to clad failure [ ms ]	86	86	87	87	87	87	86	87	87	87	87
Clad temperature at failure [ K ]	888	895	915	918	921	918	895	900	889	868	851
Clad hoop plastic strain at failure [ % ]	1.29	1.29	1.38	1.39	1.40	1.39	1.30	1.36	1.30	1.21	1.13
Clad hoop strain rate at failure [ s <sup>-1</sup> ]	0.86	0.88	0.86	0.87	0.87	0.86	0.87	0.81	0.73	0.63	0.54
Peak fuel temperature [ K ]	2499	2497	2497	2495	2494	2487	2485	2470	2435	2379	2322
Peak clad temperature [ K ]	1285	1289	1284	1290	1293	1281	1266	1251	1226	1196	1183
Peak clad hoop plastic strain [ % ]	2.77	2.98	3.10	3.23	3.33	3.33	3.30	3.13	2.83	2.40	2.07
Clad oxide thickness [ μm ]	25.1	31.1	35.0	40.6	45.8	50.6	56.5	61.6	65.9	70.4	74.1
Clad hydrogen content [ wppm ]	195	239	268	309	347	383	426	463	496	529	555
Clad fast neutron fluence [ 10 <sup>25</sup> m <sup>-2</sup> ]	4.8	5.7	6.3	7.1	7.9	8.7	9.6	10.4	11.2	12.1	12.8

Calculated best-estimate fuel rod failure conditions under the postulated PWR HZP REA are summarized in the table above. All data pertain to the rod axial segment at which clad failure is predicted to occur, i.e. to the axial position of peak power and peak clad corrosion; confer section 2.3.3. For the PWR fuel rod, this is the 9<sup>th</sup> axial segment out of 10, corresponding to an axial elevation of 2.9-3.3 m from bottom of the rod. Moreover, all data are radial average values, except for the peak fuel temperature, which is the peak value with respect to both axial and radial position in the fuel column.

## Appendix D: Calculated fuel rod failure conditions under BWR CZP CRDA

Parameter	Fuel local burnup [ MWd(kgU) <sup>-1</sup> ]								
	29.7	35.3	40.4	45.3	49.8	55.2	60.0	65.2	70.1
Peak fuel enthalpy [ J(gUO <sub>2</sub> ) <sup>-1</sup> ]	641	634	628	621	604	585	569	553	541
Time to peak fuel enthalpy [ ms ]	182	182	182	182	182	182	182	182	182
Fuel enthalpy at clad failure [ J(gUO <sub>2</sub> ) <sup>-1</sup> ]	635	625	615	604	586	573	561	547	536
Time to clad failure [ ms ]	170	168	166	164	166	168	170	172	172
Clad temperature at failure [ K ]	828	840	847	846	834	823	811	798	785
Clad hoop plastic strain at failure [ % ]	1.67	1.68	1.65	1.60	1.60	1.60	1.60	1.60	1.56
Clad hoop strain rate at failure [ s <sup>-1</sup> ]	0.35	0.39	0.45	0.48	0.42	0.36	0.30	0.25	0.23
Peak fuel temperature [ K ]	2409	2408	2407	2407	2388	2371	2352	2331	2323
Peak clad temperature [ K ]	1398	1403	1393	1401	1365	1329	1302	1279	1249
Peak clad hoop plastic strain [ % ]	3.09	3.34	3.51	3.60	3.31	3.07	2.86	2.67	2.53
Clad oxide thickness [ μm ]	11.5	13.7	15.8	17.8	19.6	21.9	24.0	26.3	28.6
Clad hydrogen content [ wppm ]	175	206	236	265	291	324	354	387	420
Clad fast neutron fluence [ 10 <sup>25</sup> m <sup>-2</sup> ]	5.0	5.9	6.8	7.6	8.4	9.3	10.1	11.0	11.8

Calculated best-estimate fuel rod failure conditions under the postulated BWR CZP CRDA are summarized in the table above. All data pertain to the rod axial segment at which clad failure is predicted to occur, i.e. to the axial position of peak power and peak clad corrosion; confer section 2.3.3. For the BWR fuel rod, this is the 6<sup>th</sup> axial segment out of 10, corresponding to an axial elevation of 1.8-2.2 m from bottom of the rod. Moreover, all data are radial average values, except for the peak fuel temperature, which is the peak value with respect to both axial and radial position in the fuel column.

## Appendix E: Calculated impact of clad corrosion on clad temperature and hoop plastic strain at failure

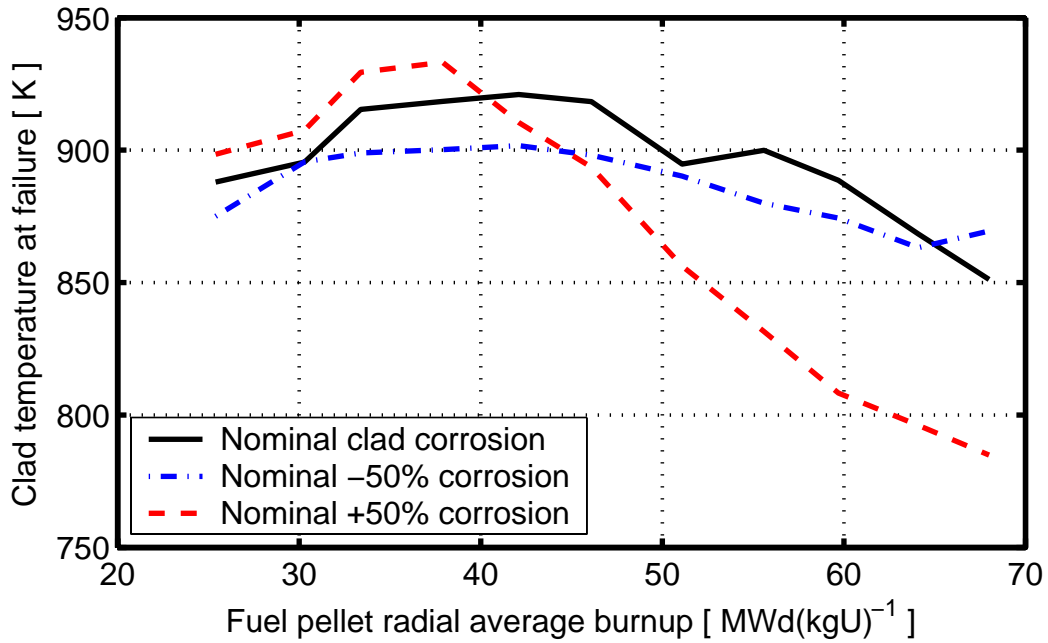


Figure E.1: Calculated clad temperature at failure (radial average value) for HZP REA, assuming a  $\pm 50\%$  variation in clad oxide layer thickness and hydrogen content.

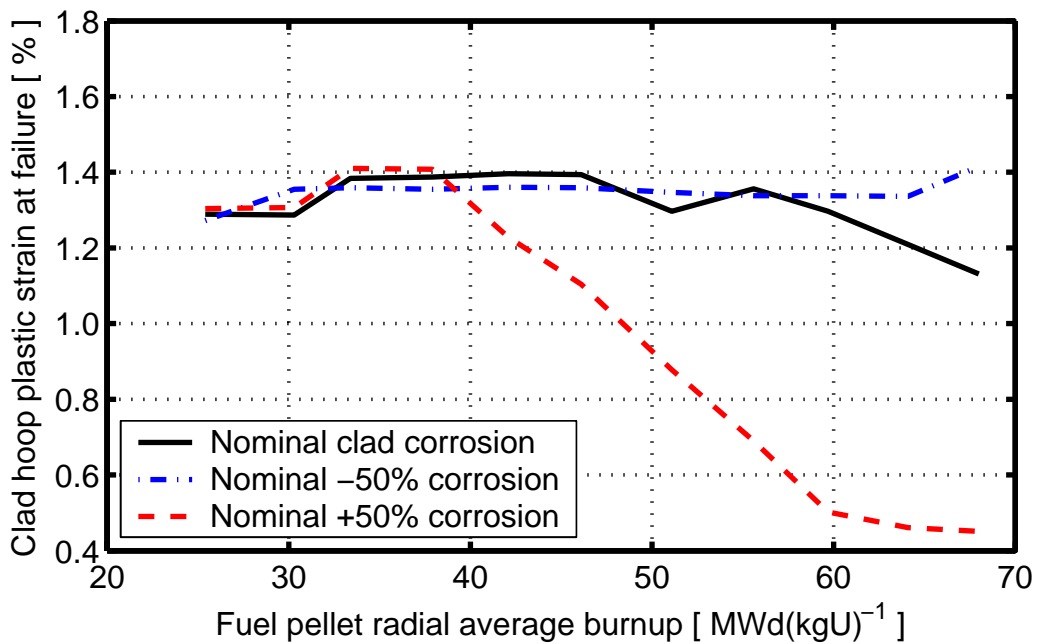


Figure E.2: Calculated clad hoop plastic strain at failure (radial average value) for HZP REA, assuming a  $\pm 50\%$  variation in clad oxide thickness and hydrogen content.

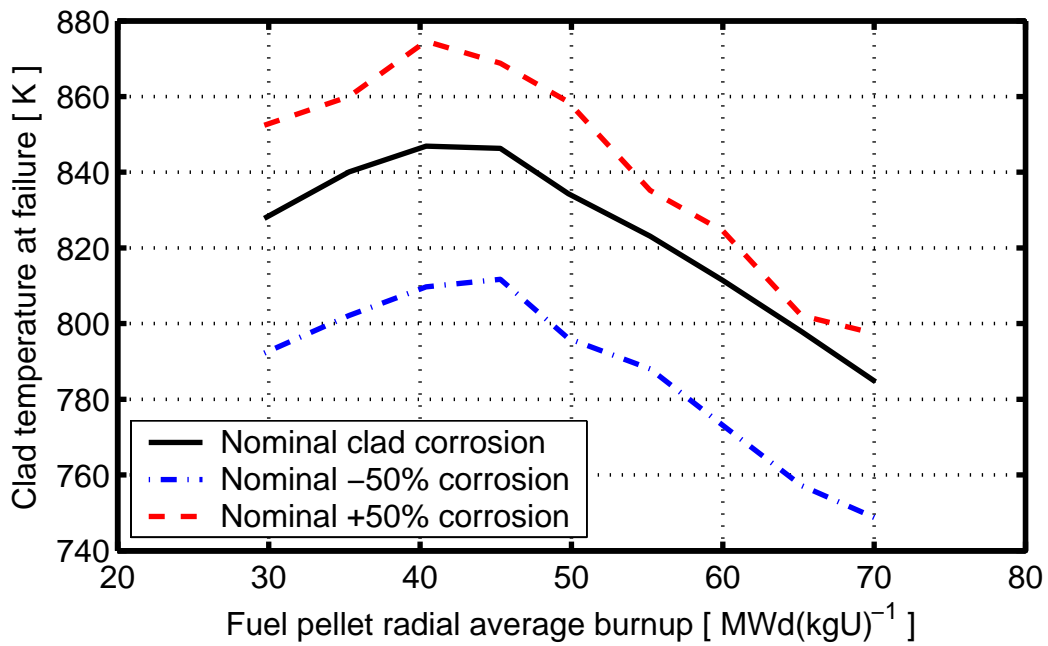


Figure E.3: Calculated clad temperature at failure (radial average value) for CZP CRDA, assuming a  $\pm 50\%$  variation in clad oxide layer thickness and hydrogen content.

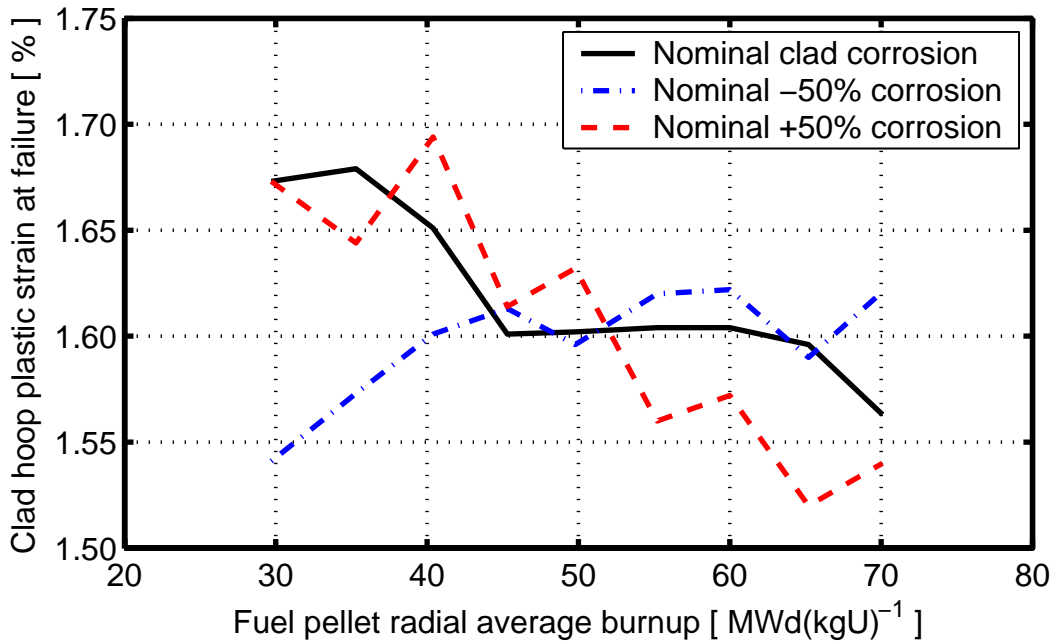


Figure E.4: Calculated clad hoop plastic strain at failure (radial average value) for CZP CRDA, assuming a  $\pm 50\%$  variation in clad oxide thickness and hydrogen content.

## Appendix F: Calculated impact of clad oxide transient spallation on clad temperature and hoop plastic strain at failure

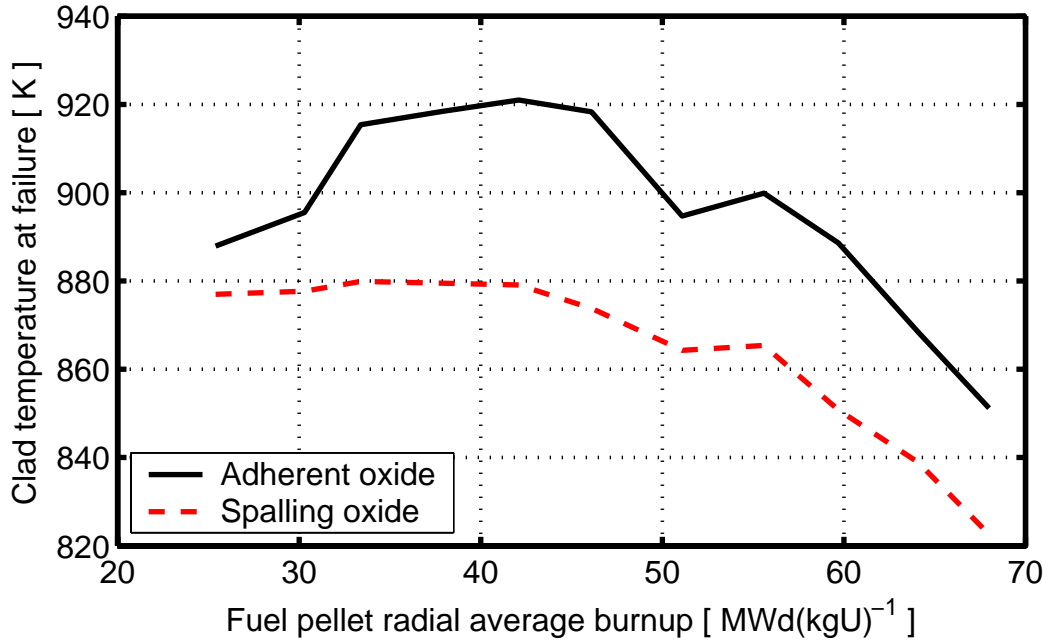


Figure F.1: Calculated clad temperature at failure (radial average value) for PWR HZP REA, assuming clad oxide spallation under the transient.

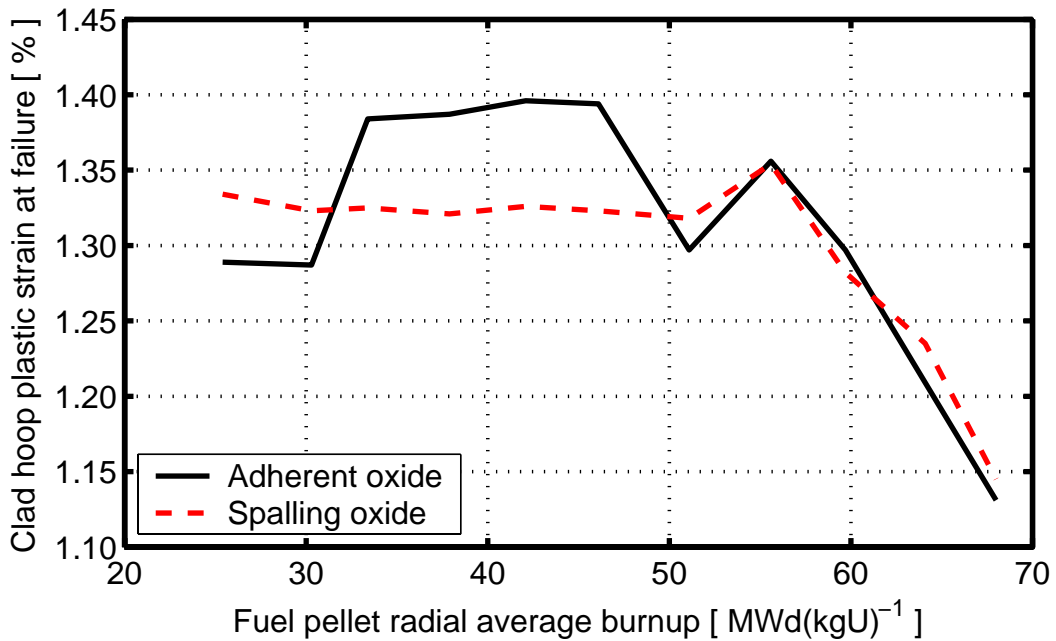


Figure F.2: Calculated clad hoop plastic strain at failure (radial average value) for PWR HZP REA, assuming clad oxide spallation under the transient.

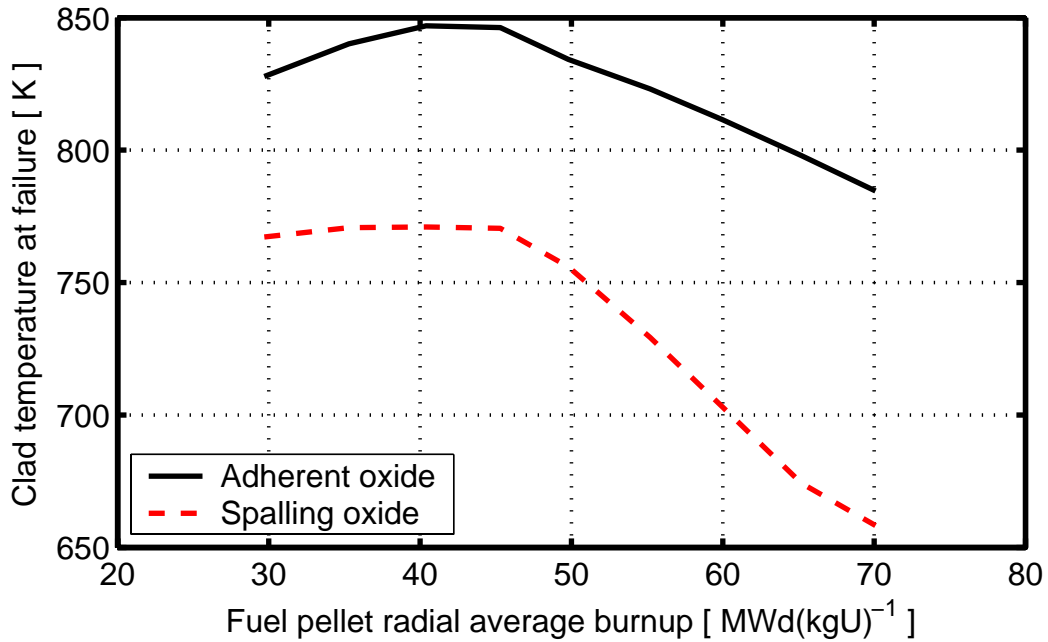


Figure F.3: Calculated clad temperature at failure (radial average value) for BWR CZP CRDA, assuming clad oxide spallation under the transient.

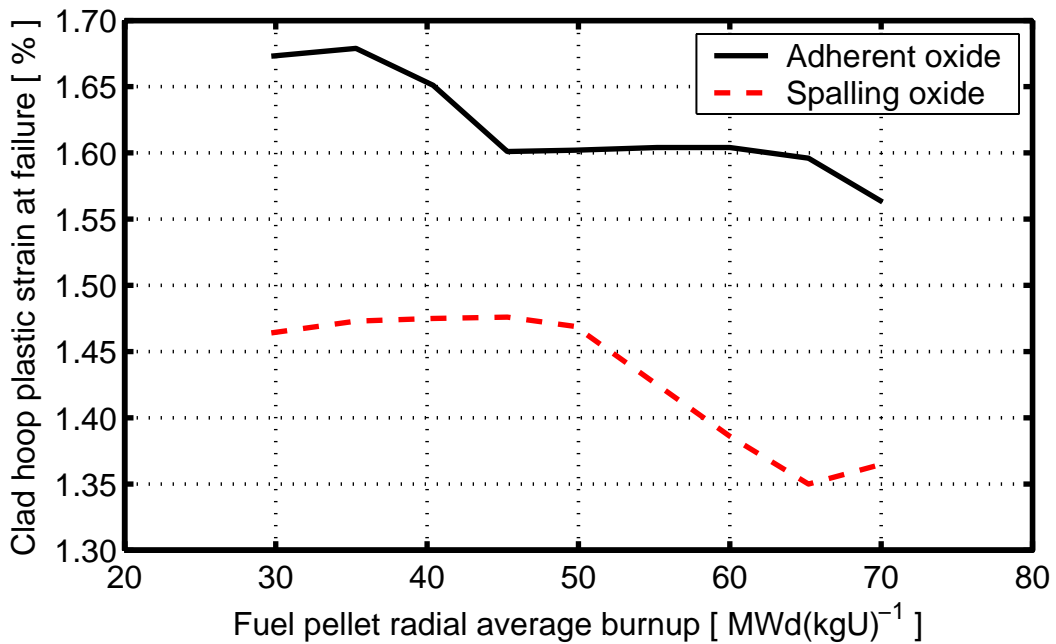


Figure F.4: Calculated clad hoop plastic strain at failure (radial average value) for BWR CZP CRDA, assuming clad oxide spallation under the transient.

[www.ski.se](http://www.ski.se)

**STATENS KÄRNKRAFTINSPEKTION**  
Swedish Nuclear Power Inspectorate

**POST/POSTAL ADDRESS** SE-106 58 Stockholm

**BESÖK/OFFICE** Klarabergsviadukten 90

**TELEFON/TELEPHONE** +46 (0)8 698 84 00

**TELEFAX** +46 (0)8 661 90 86

**E-POST/E-MAIL** [ski@ski.se](mailto:ski@ski.se)

**WEBBPLATS/WEB SITE** [www.ski.se](http://www.ski.se)